ACS OMEGA

Open Access

This article is licensed under CC-BY-NC-ND 4.0

http://pubs.acs.org/journal/acsodf

Article

Direct Liquefaction of South African Vitrinite- and Inertinite-Rich Coal Fines

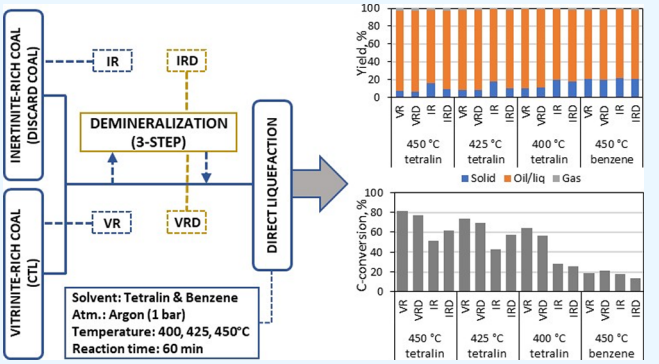
Naldo J.A. Meyer,* Christien A. Strydom, John R. Bunt, and Romanus C. Uwaoma

Cite This: *ACS Omega* 2024, 9, 12272−12289

Read Online

ACCESS | Metrics & More | Article Recommendations | Supporting Information

ABSTRACT: In this investigation, coal fines enriched with inertinite were used for direct liquefaction experiments. For comparison, a vitrinite-rich coal typically utilized in coal-to-liquid processes was also employed. To assess the impact of mineral matter content, demineralization was used to remove most of the inorganic constituents. The findings revealed that the inertinite-rich coal exhibited lower liquefaction conversions due to a reduced proportion of reactive macerals and elevated levels of inorganic mineral matter. These conversion values exhibited a strong correlation with the quantity of reactive macerals present in the parent coals. For the inertinite-rich coal, the presence of inorganic mineral matter impeded the liquefaction process but facilitated the CO_2 gasification reactions of the derived chars. To evaluate their potential in gasification processes, CO_2 gasification experiments were conducted and the reactivities and apparent gasification activation energies of both coal chars, liquefaction residue chars, and preasphaltene and asphaltene (PAA) chars were calculated. These calculations were carried out using the random pore model (RPM) and volumetric reaction model (VRM). The chemistry, reactivity, and kinetics of residue gasification conversion are not thoroughly understood, yet they hold significant importance in optimizing syngas production within gasification processes. The findings from this work highlight significant differences in liquefaction conversion values, product distribution, and composition. These differences are influenced by factors such as maceral composition, inorganic mineral matter content, hydrogen-donor capabilities of the solvent, and liquefaction reaction temperatures. Additionally, these variables affect the CO_2 gasification reactivity of liquefaction solid residue chars.



Downloaded via NORTH-WEST UNIV on April 1, 2026 at 09:06:15 (UTC).
See https://pubs.acs.org/sharingguidelines for options on how to legitimately share published articles.

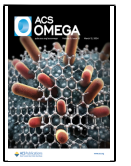
1. INTRODUCTION

South Africa, one of the leading global coal producers and exporters, plays a crucial role in the world's energy demand. The coal beneficiation process, however, leads to substantial environmental detriments, notably the generation of disadvantageous residues such as dust and fines.[1,2] The accumulation of these fines raises grave ecological concerns, including but not limited to acid mine drainage (AMD), groundwater contamination, atmospheric pollution, and susceptibility to spontaneous combustion.[1] Consequently, the coal beneficiation operations in South Africa yield substantial amounts of coal fines, around 60 Mt per annum, which are disposed of in large stockpiles, thereby precipitating noteworthy environmental predicaments.[3]

Direct coal liquefaction (DCL) involves the breakdown of a coal's macromolecular structure through the addition of a solvent under moderate temperatures and pressures, yielding liquid fuels. The resulting residues from this process are typically used in coal-to-liquids (CTL) technologies.[4] The purpose of this process is to produce hydrocarbon fuels having a hydrogen-to-carbon ratio of 1.8−2.5.[5] This is achieved through the addition of hydrogen into the system to participate in hydrogenation reactions, subsequently removing carbon and oxygen, in the form of CO, CO_2, or H_2O, from the macromolecular structure of coal. During this process, large polycyclic aromatic hydrocarbons (PAHs) are converted into smaller aromatic and/or aliphatic compounds that predominantly constitute petroleum products. The process also produces undesired products like water and gaseous hydrocarbons, including methane, ethane, and propane, that consume costly hydrogen for the generation of nontargeted compounds.[5]

The DCL process is a specific approach that incorporates hydrogenation, leading to the dissolution of coal's organic structure into soluble products.[4,6] The fundamental concept of this process is widely recognized as following the free radical mechanism. This mechanism involves the cleavage or cracking of coal molecules, yielding fragments that are commonly

Received: January 18, 2024
Revised: January 24, 2024
Accepted: January 29, 2024
Published: February 29, 2024



© 2024 The Authors. Published by American Chemical Society

Table 1. Characterization of the Coal and Demineralized Coal Samples[a]

properties	method of analysis	VR	VRD	IR	IRD
Proximate Analysis (wt %, a.d.)					
% inherent moisture content	ISO 11722:1999	7.6	2.9	4.5	2.9
% ash yield	ISO 1171:2010	12.4	0.7	28.3	1.1
% volatile matter	ISO 562:2010	31.8	35.8	23.8	29.2
% fixed carbon	by difference	48.2	60.6	43.4	66.8
fuel ratio	FC/VM	1.5	1.7	1.8	2.3
gross calorific value (MJ kg^{-1})	ISO 1928:2009	25.4	29.6	20.3	28.5
Ultimate Analysis (wt %, d.a.f.)					
% carbon content	ISO 17247:2013	77.9	77.8	77.3	77.8
% hydrogen content	ISO 17247:2013	5.5	5.0	4.6	3.8
% nitrogen content	ISO 17247:2013	2.1	2.2	2.0	2.1
% oxygen content	by difference	13.7	14.4	14.9	15.4
% total sulfur	ISO 19579:2006	0.7	0.6	1.2	0.8
O/C molar ratio		0.132	0.139	0.145	0.149
H/C molar ratio		0.842	0.759	0.706	0.586
maceral composition (vol %)	ISO 7404-3				
% vitrinite		72.2	-	37.0	-
% liptinite (exinite)		3.9	-	0.7	-
% reactive semifusinite		5.3	-	24.9	-
% inert semifusinite		8.7	-	15.7	-
% fusinite + secretinite		3.1	-	6.3	-
% mineral matter (calculated)		6.8	-	15.4	-
total reactives (m.m.f.)		81.4	-	62.6	-
total inerts (m.m.f.)		18.6	-	37.4	-
vitrinite classification content		mod. high	-	low	-
Rank and Vitrinite Reflectance					
rank determination	ISO 11760	med C	-	med C	-
RoV max	ISO 7404-5	0.62	-	0.68	-

[a]a.d. = Air-dried; d.a.f. = dry ash-free; m.m.f. = mineral matter-free.

referred to as free radicals. These free radicals then undergo hydrogenation, facilitated by the presence of hydrogen, leading to the formation of lighter products such as oil and gas. Conversely, under conditions where the availability of hydrogen for donation is insufficient, the larger radicals tend to condense through undesirable repolymerization and recombination reactions, resulting in the formation of unwanted residues such as tars and cokes containing large, unreactive polycyclic aromatic structures.[5,7,8] In addition to the solvent's most crucial role in hydrogen donation, the solvent acts as a carrier for coal particles and facilitates heat transfer.[5,8] This transformation of the macromolecular network occurs at moderate temperature and pressure, typically within the range of 400−455 °C and at 69−172 bar, facilitated by the presence of a solvent.[5,6,9] High pressures in coal liquefaction processes are applied to accelerate reactions, enhance solubility, allow cracking of molecules, minimize gas production, increase yields, and improve the quality of the resulting liquid products.[10] The solubilized products, which are predominantly comprised of aromatic compounds, can be further upgraded using conventional petroleum refining methods, such as hydrotreating, to meet the final specifications of liquid products.[6,8,11]

Coal liquefaction plays an important role in the production of liquid fuels and other petroleum products, particularly for countries lacking crude oil reserves like South Africa. Notably, liquefaction solid residues account for approximately one-third of the coal input, and their utilization is important in reducing the overall cost of the liquefaction process.[7,12] Managing the solid waste generated by the chemical industry has gained much attention, with coal liquefaction residues representing about 25−30% of the feed coal.[12] The residues generated through liquefaction comprise not only unreacted coal macerals and intrinsic mineral components but also residual oil, as well as asphaltenes and preasphaltenes (PAAs).[13] Employing thermal conversion through gasification presents an economically viable solution to improve the process output. Nevertheless, the high moisture contents of such feedstocks pose technical and conversion efficiency limitations on direct gasification. To address these challenges and enhance feedstock properties such as energy density and structural features, hydrothermal carbonization serves as a viable pretreatment method.[12] These residues contain significant amounts of carbon, hydrogen, inorganic substances, and spent catalysts. Increasing concerns are emerging regarding the disposal of residues and their detrimental environmental impact. Therefore, both economic and environmental considerations will encourage the recovery of higher-value, lighter products from direct liquefaction residues. The aspiration here is to produce valuable carbon products through residue conversion that can be effectively utilized.[4,13] Gasification of these residues offers the potential to produce syngas, a versatile intermediate used in the production of liquid fuels and chemicals through Fischer−Tropsch (FT) synthesis. Moreover, if hydrogen (H_2) is separated from the syngas, it can be reused in the DCL process to hydrogenate the recycled solvent, thus reducing operational costs.[14]

In this investigation, coal liquefaction experiments of South African vitrinite- and inertinite-rich coal were conducted in an autoclave reactor under an inert atmosphere utilizing tetralin as

https://doi.org/10.1021/acsomega.4c00602
ACS Omega 2024, 9, 12272−12289

a hydrogen donor solvent at 400, 425, and 450 °C. The product yield fractions were quantitatively and qualitatively examined using standard and advanced analytical techniques. In addition, the gasification reactivities of the coals and resultant residue chars were examined using thermogravimetric analysis (TGA). Proximate and ultimate analyses, Fourier transform infrared spectroscopy (FTIR), surface area characterization, and X-ray diffraction (XRD) analyses of the residues were performed to characterize the properties of the residues and evaluate their roles during CO_2 gasification. These results will determine the potential uses of liquefaction solid residues in gasification processes. Furthermore, the effect of mineral matter contents during the gasification of the coal and liquefaction residue chars was evaluated by demineralization methods.

2. EXPERIMENTAL SECTION

2.1. Materials. Highveld inertinite-rich fine coal filter cake (IR) and a seam 4 vitrinite-rich (VR) coal from the Witbank coalfields (a typical coal used in coal to liquid processes in South Africa) were used as the raw feed material in this study. The pulverized (−300 μm) samples were dried at 100 °C for 24 h to reduce the inherent moisture content in the samples. Both coals were classified as bituminous medium rank C coals. The coal samples were characterized using the methods summarized in Table 1.

Table 1 presents the results and methods used for proximate and ultimate analyses, calorific values, maceral composition, and rank determination. Demineralization experiments (as described in Section 2.2) were conducted on the two coal samples to evaluate the effect of minerals during liquefaction experiments. The analysis results for the demineralized samples are also included in Table 1 and are denoted as VRD (demineralized vitrinite-rich coal) and IRD (demineralized inertinite-rich coal).

X-ray fluorescence (XRF) spectroscopic analysis was conducted on the ash derived from the two raw coals using a PANalytical (Axios Max) WD-XRF spectrometer and is presented in Table 2. These results are presented as elemental oxides on loss on an ignition-free basis. From the normalized XRF data, the alkalinity indices (*AI*) were determined using eq 1:

Table 2. Ash Composition of the VR and IR Coals Presented as Mineral Oxides

XRF results (wt %, LOI-free basis)	VR	IR
SiO_2	62.3	49.9
Al_2O_3	25.5	27.9
CaO	3.0	7.3
Fe_2O_3	3.2	4.6
K_2O	1.1	1.2
MgO	1.5	1.8
MnO	n.d.	0.1
Na_2O	0.1	0.3
P_2O_5	0.1	0.8
TiO_2	1.4	1.4
SO_3	1.8	4.9
alkalinity index (AI)	1.3	5.4
$SiO_2 + Al_2O_3 + Fe_2O_3$	91.1	82.3

$$AI_1 = \text{Ash yield} \times \left(\frac{Fe_2O_3 + CaO + MgO + Na_2O + K_2O}{SiO_2 + Al_2O_3 + P_2O_5} \right) \quad (1)$$

The provided expressions for alkali indices serve the purpose of providing insight into the catalytic effects of diverse minerals present in the coal ash when undergoing conversion processes. Within these expressions, the catalytic impact can be assumed through the alkali index, which is established as the ratio between the cumulative weight percentages of inorganic elements (expressed as elemental oxides) exhibiting catalytic tendencies (K_2O, CaO, MgO, Na_2O, and Fe_2O_3) and those with inhibitory tendencies (SiO_2, Al_2O_3, and P_2O_5).[15] Furthermore, the equation incorporates a factor involving the ash yield, multiplying it by this ratio, to accommodate coals with both high and low ash concentrations.

2.2. Demineralization Experiments. To consider the effect of inorganic minerals on the liquefaction process, acid treatment was conducted on the vitrinite-rich (VR) and inertinite-rich (IR) coal samples using concentrated hydrochloric acid (32%) and hydrofluoric acid (48%) to remove most of the inorganic components. Adapted from Strydom et al.,[16] a three-step, 24-h treatment process was employed using a coal-to-acid weight ratio of 1-to-3. The treatment involved continuous stirring and subsequent filtration to isolate the acidic solution from the solid carbon-rich material. The sequence of acids used was HCl, followed by HF, and concluding with another round of HCl. Following the third treatment, the carbon-rich material underwent washing with Milli-Q water until reaching a pH level of at least 6. The demineralization method's efficiency was quantified by assessing the demineralization efficiency, E_d, expressed as a percentage. To determine the achieved demineralization efficiency, E_d, the following formula was employed[13]:

$$E_d = \left(\frac{A_0 - A_d}{A_0} \right) \times 100\% \quad (2)$$

where A_0 is the ash yield of the coal before demineralization, and A_d is the ash yield of the demineralized coal. The demineralization experiments yielded demineralization efficiencies of 94.4 and 96.1% for the vitrinite-rich (VR) and inertinite-rich (IR) coal samples, respectively.

2.3. Liquefaction Experiments. The liquefaction experiments were carried out using a 600 mL stainless steel autoclave reactor (Parr Instruments, US), controlled using a 4848 controller from Parr. The feed materials were mixed with tetralin (1,2,3,4-tetrahydronaphthalene for synthesis; ≥ 98%), a hydrogen-donor organic solvent, and benzene (ReagentPlus; purity ≥99%), a hydrogen-poor organic solvent, to a 1-to-3 weight ratio. An initial pressure of 0.2 MPa (2 bar) (absolute pressure), measured using a pressure display module integrated into the reactor controller, was applied by introducing an inert argon (AFROX, 99.999%) atmosphere. The temperature of the reaction vessel was increased to 450 °C at 10 °C/min with an isothermal reaction time of 60 min. To ensure thorough mixing of the reacting materials and solvent during the experiment, the stirrer speed was set to 250 rpm. After the reaction period, the reaction vessel was cooled to room temperature using an internal cooling coil controlled by a solenoid valve module. Once the temperature attained room temperature, the gas fraction was collected in a 5 L Tedlar gas

https://doi.org/10.1021/acsomega.4c00602
ACS Omega 2024, 9, 12272−12289

bag and set aside for analysis. The liquid and solid products were removed from the reactor vessel and separated using dichloromethane as the solvent and vacuum filtration to obtain the solid residue fraction. The dichloromethane was removed from the liquid yield using rotary evaporation. N-hexane was added to the liquid product and heated to 85 °C for 60 min.[17] The solution was vacuum-filtered to further separate the liquid product into *n*-hexane soluble fractions as the oil yield and *n*-hexane insoluble fractions as the asphaltenes and preasphaltenes (PAA). The oil was isolated by removing the *n*-hexane using rotary evaporation. Three replicates of the liquefaction experiments were performed, and the standard deviations of the yields were determined to be less than 2%.

The following equations were used to calculate the weight percentages of the solid residues (W_{SR}), preasphaltenes and asphaltenes (W_{PAA}), liquid/oil residues (W_{liq}), and gas yield (W_{gas}):

$$W_{SR} = \left(\frac{m_{SR}}{m_{sol} + m_{feed}}\right) \times 100\% \quad (3)$$

$$W_{PAA} = \left(\frac{m_{PAA}}{m_{sol} + m_{feed}}\right) \times 100\% \quad (4)$$

$$W_{liq} = \left(\frac{m_{liq} - m_{PAA}}{m_{sol} + m_{feed}}\right) \times 100\% \quad (5)$$

$$W_{gas} = 100\% - W_{SR} - W_{liq} - W_{PAA} \quad (6)$$

where m_{sol} and m_{feed} represent the mass (in grams) of the solvent and feed material, respectively; and m_{SR}, m_{PAA}, and m_{liq} represent the mass (in grams) of the solid residues, preasphaltenes and asphaltenes, and liquid/oil residues, respectively. All masses are presented on a dry and ash-free basis. The carbon conversions, C_{daf}, of the feed materials during solvent extraction were calculated on a dry, ash-free basis using the following equation and are presented as a percentage:

$$C_{daf} = \left[\frac{m_{feed} - m_{SR}}{m_{feed}}\right] \times 100\% \quad (7)$$

Carbon conversion values were calculated to determine the percentage of feed material that reacted to produce the liquid and gaseous products during liquefaction processes.

2.4. Characterization of Feed Materials and Residues.

2.4.1. Proximate Analysis, Ultimate Analysis, and Calorific Values. The coal samples, demineralized coal samples, and solid residues were subject to proximate analysis, ultimate analysis, and calorific value determinations using the methods highlighted in Table 1, while the proximate analysis of the PAA products was approximated using thermogravimetric analysis (to follow in eqs 13−16). The results from the approximated proximate analysis were used to determine the approximate higher heating values (HHV) of the solid residues and PAA obtained from the liquefaction experiments using eq 8[18]:

$$\mathrm{HHV(MJ\ kg^{-1})} = 0.3536\,\mathrm{FC} + 0.1559\,\mathrm{VM} - 0.0078\,\mathrm{ASH} \quad (8)$$

where the fixed carbon content, volatile matter content, and ash yield are represented by FC, VM, and ASH, respectively.

2.4.2. CO_2 Low-Pressure Adsorption Analysis. The CO_2 low-pressure adsorption analysis, also known as CO_2-LPGA, was performed on the coal and demineralized coal samples, and their respective solid residues and PAA products using a Micrometics ASAP 2010 instrument. The method of analysis is reported elsewhere.[19] The micropore surface area of the samples was determined from the CO_2 adsorption data using the Dubinin−Radushkevich (D−R) method.[19,20] The maximum micropore volume, average micropore diameter, and pore size distribution (PSD) were calculated using the CO_2 adsorption data following the H−K method.[19,21,22] These calculations were based on the entire isotherms within the reduced pressure ranges. The H−K method, a modification of the Kelvin equation, considers pore filling by the liquid phase of the adsorbate rather than the formation of a gaseous phase adsorbate layer. It also takes into account the dimensions of slit-shaped pores.[19,22] This method provides a realistic micropore PSD in the lower pressure range ($0.06 \leq P/P_0 \leq 0.07$). The purpose of the CO_2 low-pressure gas adsorption was to determine the surface area and porosity of the coal samples, demineralized materials, and their respective liquefaction solid residues and PAA.

2.4.3. FTIR Spectroscopy. Fourier-transform infrared spectroscopy, FTIR, was employed for the characterization of solid materials and residues. A BRUKER ALPHA-P attenuated total reflection Fourier-transform infrared spectrometer was utilized for solid-state analyses. OPUS version 6.0 (BRUKER software) was used for spectrum acquisition and processing. The FTIR spectra were captured with a wavelength range of 4000−400 cm^{-1}.

2.4.4. X-ray Diffraction. Qualitative and quantitative XRD analyses were conducted on the coal and demineralized coal samples and their respective solid residues and PAA to evaluate fractions of minerals and amorphous phases contained in the samples. Diffractograms were obtained for the different materials and products using a Malvern PANalytical Aeris diffractometer with a PIXcel detector and fixed slits with Fe-filtered Co-Kα radiation. The phases were identified using X'Pert Highscore Plus software. The relative phase amounts (weight %) were estimated using the Rietveld method.[23] Curve-fitting manipulation was applied to obtain three Gaussian peaks that were used to fit XRD patterns at around 20, 29, and 50°. These were assigned as γ, 002, and 100 bands, respectively.[24] When considering that the interlayer structure of coal has a uniform density, Hirsch[25] evaluated the molecular structure of pulverized coal using XRD analysis to determine the interlayer spacing (d_{002}), stacking heights (L_c), and average lateral sizes (L_a) of the crystallite structures (eqs 9−11):

$$d_{002} = \frac{\lambda}{2\sin\theta_{002}} \quad (9)$$

$$L_c = \frac{0.89\,\lambda}{\beta_{(002)} \times \cos\theta_{(002)}} \quad (10)$$

$$L_a = \frac{1.84\,\lambda}{\beta_{(100)} \times \cos\theta_{(100)}} \quad (11)$$

$$n = \frac{L_c}{d_{002}} \quad (12)$$

where λ is the X-ray wavelength equal to 1.789 nm, and the diffraction angles, θ_{002} and θ_{100}, correspond to the 002 and 100

https://doi.org/10.1021/acsomega.4c00602
ACS Omega 2024, 9, 12272−12289

peak positions, respectively. The fwhm (full width at half-maximum) of the 002 and 100 peaks are represented as β_{002} and β_{100}, respectively.[25] The stacking number of aromatic layers are signified by n in eq 12.[24,26]

2.4.5. Pyrolysis of Solid Fractions. Pyrolysis experiments of the coal, demineralized coal, and residues were conducted using an SDT Q600 TGA instrument from TA Instruments. The results show the relationship between mass loss and temperature as a result of decomposition and dehydration reactions on a mass loss (%) versus temperature (°C) plot and its derivative (%/°C) as a function of temperature in a differential thermal gravimetric analysis (DTG) plot. Approximately 15 mg (±1 mg) of the sample was loaded in a 90 μL alumina crucible and subject to thermogravimetric analysis. An inert environment was created using nitrogen (AFROX, 99.999%) with a constant flow rate of 100 mL/min. The samples were heated from 25−960 °C with a linear heating rate of 20 °C/min.[13,27]

Additionally, moisture content ($MC_{approx.}$), ash yield ($ASH_{approx.}$), volatile matter content ($VM_{approx.}$), and fixed carbon content ($FC_{approx.}$) were approximated from the pyrolysis and gasification (Section 2.4.6) results with a <2% difference when compared to proximate results obtained using the ISO methods (ISO 11722; ISO 1171; ISO 562). The approximate proximate analysis was calculated using eqs 13−16:

$$MC_{approx.} = \frac{m_i - m_{180\,^\circ C}}{m_i} \times 100\% \quad (13)$$

$$ASH_{approx.} = \frac{m_{ash}}{m_i} \times 100\% \quad (14)$$

$$VM_{approx.} = \frac{m_{180\,^\circ C} - m_{char}}{m_i} \times 100\% \quad (15)$$

$$FC_{approx.} = \frac{m_{char} - m_{ash}}{m_i} \times 100\% \quad (16)$$

where m_i, $m_{180\,^\circ C}$, m_{ash}, and m_{char} denote the initial sample mass at 25 °C, mass at 180 °C, mass of the ash after full conversion, and the mass of the char prior to CO_2 gasification at 960 °C, respectively. The approximate HVVs (in MJ kg^{-1}) were calculated from these results using eq 8.

2.4.6. Char-CO_2 Gasification and Kinetics. CO_2 gasification experiments were conducted on the chars of the coal samples and demineralized coal samples and their respective liquefaction solid residues and PAAs using an SDT Q600 thermogravimetric analyzer from TA Instruments. The samples were heated to the desired isothermal reaction temperature (900, 930, and 960 °C) at 20 °C/min in an inert atmosphere (as discussed in Section 2.4.5) to remove residual volatile contents before gasification tests. When the desired isothermal temperatures were reached, the atmosphere was switched to CO_2 with a 30 mL/min flow rate until the reaction was completed and full conversion was reached. The reactivity at 50 and 90% ($R_{0.5}$ and $R_{0.9}$) conversion was calculated using eqs 17 and 18, where t is the time at conversion in minutes. The fractional carbon conversions (X), initial reactivities (R_i), and average final reactivities (R_{fa}) were evaluated using eqs 19−21[7,13]:

$$R_{0.5} = \frac{0.5}{t_{0.5}} \quad (17)$$

$$R_{0.9} = \frac{0.9}{t_{0.9}} \quad (18)$$

$$X = \frac{m_0 - m_t}{m_0 - m_{ash}} \quad (19)$$

$$R_i = \left.\frac{dX}{dt}\right|_{X=0.1} \quad (20)$$

$$R_{fa} = \frac{\sum_{X=0.9}^{X=0.7} \frac{dX}{dt}}{N} \quad (21)$$

where X is the fractional carbon conversion, m_0 is the initial mass of the char before gasification, m_t is the mass of the char at reaction time (t), m_{ash} is the mass of the residual ash remaining after gasification occurred, and N in the number of data points.

Two gasification reaction kinetic models were used to perform the kinetic modeling and calculation of kinetic parameters for the gasification process of the samples. These models include the random pore model (RPM) and the volumetric reaction model (VRM). The random pore model (RPM) considers a random distribution of pore sizes and orientations. Unlike other models, the RPM specifically accounts for the structural changes in the char as the reaction progresses. The liquefaction process affects the pore structure of the coal matrix, and these alterations have a significant impact on the advancement of the reaction. Equation 22 provides the expression for the overall reaction rate using the random pore model (RPM).

$$\frac{dX}{dt} = \frac{r_s S_0 (1 - X)\sqrt{1 - \psi \ln(1 - X)}}{(1 - \varepsilon_0)} \quad (22)$$

The intrinsic reaction rate, denoted as r_s, considers the impact of the operating conditions. S_0 and ε_0 are the pore surface area and solid porosity, respectively. To address variations in the char's structure during the progression of the gasification reaction, a dimensionless structural parameter (Ψ) is introduced which is determined by char properties, as specified in eq 23:

$$\psi = \frac{4\pi L_0 0(1 - \varepsilon_0)}{S_0^2} \quad (23)$$

where L_0 is the pore length. The RPM gasification conversion fraction (X) at the gasification reaction time, t, is determined using eq 24, where the time factor (t_f) is evaluated using the random pore model.

$$X = 1 - \exp\left[- t_f t \times \left(1 + \frac{t_f t \psi}{4}\right)\right] \quad (24)$$

The structural parameter, Ψ, can be estimated through linear regression using the dimensionless reduced time, $t/t_{0.9}$ (eq 25):

$$\frac{t}{t_{0.9}} = \frac{\sqrt{1 - \psi \ln(1 - X)} - 1}{\sqrt{1 - \psi \ln(1 - 0.9)} - 1} \quad (25)$$

The activation energy, denoted as E_a, was determined by calculating the slope of the graphical representation of $\ln(t_f)$ plotted against T^{-1}. Concurrently, the lumped pre-exponential factor, denoted as k_{so}, was approximated from the intercept from the $\ln(t_f)$ versus T^{-1} plot.

https://doi.org/10.1021/acsomega.4c00602
ACS Omega 2024, 9, 12272−12289

$$\ln(t_f) = -\frac{E_a}{RT} + m\ln(y_{CO_2}) + \ln(k'_{SO}) \quad (26)$$

The quality of fit (QOF) was evaluated by fitting the kinetic models and applying eq 27:

$$\text{QOF}\ (\%) = 100 \times \left(1 - \frac{\sum_1^N \frac{X_{cal} - X_{exp}}{X_{exp}}}{N}\right) \quad (27)$$

where X_{cal} and X_{exp} are determined from the calculated and experimental conversion values obtained from the models, respectively. The number of data points used for the models is represented by N.

The volumetric (homogeneous) reaction model (VRM) assumes that gasification reactions take place homogeneously throughout the inner and outer surfaces of the reaction environment. The volumetric reaction model was proposed by Wen[28]:

$$X = 1 - \exp(-t_f t) \quad (28)$$

where t_f is the time factor determined using the volumetric reaction model (VRM). The apparent activation energies determined using R_i, R_{fa}, $R_{f0.5}$, and $R_{f0.9}$ were calculated by plotting the ln of the reactivity value against $1/T$ (K^{-1}).

2.5. Characterization of Liquid Products from Liquefaction Experiments. *2.5.1. GC-MS and Calorific Values of Liquid Products.* Gas chromatography−mass spectrometry (GC-MS) analyses were conducted to characterize the liquid products obtained from the coal liquefaction experiments. An Agilent 6890N gas chromatograph (GC) coupled with an Agilent 5975 mass detector was utilized for this purpose. The GC instrument was equipped with an Agilent 19091S column, with a length of 30 m, a diameter of 0.25 mm, and a film thickness of 0.25 μm. The column temperature was programmed to increase at a rate of 5 °C/min until it reached 290 °C. Once the desired temperature was reached, it was maintained isothermally for 30 min to ensure complete evolution of all sample components. For peak identification, the National Institute of Standards and Technology (NIST) database was employed. This database served as a reference for identifying the peaks obtained during the GC-MS analysis, aiding in the characterization of the samples. In addition, FTIR spectroscopic analysis was conducted using the method previously mentioned (Section 2.4.3).

2.6. Gas Composition Using Gas Chromatography. For further gas analysis, a PerkinElmer Clarus 500 Gas Chromatograph was used, with two columns (Agilent J&W HP-PLOT/Q 30 m × 0.535 mm and PerkinElmer Elite GC GS MSIEVE 30 m × 0.53 mm) interconnected to the injector and detector via a VICI 10-port gas sampling valve from Valco Instruments. The detector (TCD, thermal conductivity detector) was set to 100 °C, and the gas samples were injected using a capillary injector operating at the same temperature. Argon, supplied by AFROX with a purity of 99.999%, served as the carrier gas at an initial flow rate of 2 mL/min, increasing to 8 mL/min after 16 min. The oven temperature was set to 40 °C, and the GC system was calibrated for CO_2, CO, H_2, CH_4, C_2H_6 O_2, and N_2 analysis. A 1 mL gas sample was injected, with CO_2 being separated out in the PLOT Q column, and a valve switch preventing it from entering the MSIEVE column. The concentration of each component was determined using the peak areas in the chromatogram. Data processing is conducted using TotalChrom Navigator software designed for the Clarus 500 GC.

The change in total pressure is attributed to the increase in partial pressures of the gases produced. By monitoring the change in pressure and knowing the initial pressure and the properties of the gases involved, the amount of gas produced may be quantified. Dalton's law was used to determine the partial pressures of the individual gas components together with the volume or molar percentage from gas chromatography. Dalton's law states that the total pressure exerted by a mixture of nonreacting gases is the sum of the partial pressures of each individual gas: $P_{total} = P_1 + P_2 + ... + P_n$, where P_{total} = Total pressure of the gas mixture, and P_1, P_2, ..., P_n = Partial pressures of individual gases in the mixture. Lastly, the ideal gas law (PV = nRT) was used to calculate the number of moles of each gas species in the mixture at a specific temperature (25 °C) and pressure. From the number of moles of each gas, the mass could be determined.

3. RESULTS AND DISCUSSION

3.1. Liquefaction Product Distribution. Initial liquefaction pressures, with tetralin as solvent, at the reaction temperatures of 400, 425, and 450 °C ranged between 20 and 23 bar, 27 and 31 bar, and 38 and 40 bar, respectively. The pressures of the experiments conducted using benzene as the solvent at 450 °C ranged between 65 and 69 bar. At 450 °C, the pressures at the end of the reaction period ranged between 43 and 48 bar using tetralin and between 72 and 76 bar using benzene. Table S5 highlights the partial pressures of the gas yields at the end of the reaction period and cooled down to 25 °C. These pressures are directly proportional to the mass of the gases produced from the process. The reaction pressures obtained from tetralin liquefaction were lower than the typical pressures used in DCL processes, which ranged between 69 and 155 bar.[6] This is due to the initial volume occupation of the feed material and solvent. Higher reaction pressures can be obtained by increasing the amount of solvent used, or by increasing the initial argon pressure.

Tetralin, a hydrogen donor solvent, together with benzene, a hydrogen-poor solvent, was used to evaluate the liquefaction effectiveness and product quantity and quality produced with two aromatic solvents with different hydrogen-donor capabilities. Table 3 shows the product yields of the VR, VRD, IR, and IRD coal produced from liquefaction experiments conducted at 400, 425, and 450 °C using tetralin. In addition, product yields of liquefaction experiments conducted in benzene at 450 °C were included. The results from the experiments conducted at 425 and 400 °C have shown low conversion values (5−10% conversion) and were excluded from this study. For tetralin liquefaction at 450 °C, carbon conversion values of 81.0, 77.0, 50.9, and 61.7% were obtained from the VR, VRD, IR, and IRD coals, respectively. The overall conversion of the IR coal is lower than that of the VR coal by 30.9, 31.4, and 35.7% at 400, 425, and 450 °C, respectively. Uwaoma et al.[17] found similar conversion values during tetralin liquefaction of density-separated fractions derived from Highveld coal fines. The difference between these conversion values can predominantly be ascribed to the different maceral compositions of the two coals. The fractions of reactive macerals, namely, vitrinite and exinite, are significantly higher in the VR coal compared to the IR coal with vitrinite contents of 72.2 and 37.0% and exinite contents of 3.9 and 0.7%,

https://doi.org/10.1021/acsomega.4c00602
ACS Omega 2024, 9, 12272−12289

Table 3. Liquefaction Product Distribution of Experiments Conducted at 400, 425, and 450 °C with Tetralin as the Solvent and at 450 °C with Benzene as the Solvent[a]

	yield, weight % (d.a.f.)			
sample	solid residue	liquid residue	gas	carbon conversion, % (d.a.f.)
VR 450t	4.1	93.4	2.5	81.0
VRD 450t	5.5	91.8	2.6	77.1
IR 450t	9.0	89.0	2.0	50.9
IRD 450t	9.1	88.1	2.8	61.7
VR 425t	5.6	92.3	2.1	73.8
VRD 425t	7.5	90.3	2.3	69.1
IR 425t	10.7	88.0	1.3	42.4
IRD 425t	10.0	87.6	2.4	57.2
VR 400t	7.7	91.5	0.8	63.9
VRD 400t	10.5	88.4	1.1	56.7
IR 400t	13.3	85.7	1.0	28.2
IRD 400t	17.6	80.6	1.8	25.8
VR 450b	17.6	80.3	2.2	18.5
VRD 450b	19.2	78.8	2.0	21.1
IR 450b	15.0	83.9	1.1	17.7
IRD 450b	20.4	78.0	1.6	13.4

[a]Feed materials = VR, VRD, IR, IRD; Liquefaction temperatures = 400, 425, 450 °C; Solvent used: t = tetralin, b = benzene; feed-to-solvent = 25:75.

respectively, while reactive semifusinite contents were 5.3 and 24.9%, respectively (Table 1). Similar observations were also made by Yan et al.[7] Inertinite macerals contain less aliphatic and oxygen-containing functional groups, making the nature of the coal's macromolecular structure more aromatic.[29] The lower H/C molar ratio of the IR coal compared to the VR coal can be attributed to the higher degree of aromaticity (Table 1). The IR coal comprises more inertinite that is difficult to convert during the liquefaction process and will most likely remain in the solid residue fraction. The results from Table 3 support this statement. Higher oil yields derived from the liquefaction experiments of the VR coal are accompanied by higher carbon conversion at all temperatures. While the alkali indices for IR coal are high and catalytic effects may be anticipated, the results show that the high ash yield in IR coal inhibits liquefaction conversion reactions when compared to its demineralized counterpart, IRD. However, the VR coal resulted in higher conversion values than its demineralized counterpart, VRD, indicating that catalytic effects may be caused by its inorganic constituents. Certain minerals are known for their definite catalytic effects during gasification, while others are noted for their catalytic effects in liquefaction.[10,30] In addition, it is widely acknowledged that higher temperatures also promote the breakdown of coal macromolecules.[10,27,31,32] The resulting fragments and radicals undergo hydrogenation through active hydrogen interactions, leading to the creation of oil or hydrocarbon gases. This process is contingent on the availability of ample active hydrogen atoms or hydrogen radicals, typically sourced from a hydrogen donor solvent such as tetralin.[10] Consequently, increased temperatures elevate the production of oil and gas.

Liquefaction experiments performed at 450 °C utilizing benzene, an H-poor aromatic solvent, exhibited inefficacy, resulting in lower conversion values (<22%) in contrast to the 400−450 °C tetralin experiments. These findings underscore the necessity of a hydrogen-donating solvent in coal liquefaction, independent of coal's molecular composition. It is worth noting that supercritical conditions were achieved with both solvents. Consequently, the primary emphasis of this study will be on examining the liquefaction outcomes derived from experiments conducted with tetralin as the selected solvent.

During solvent extraction using *n*-hexane to remove the preasphaltene and asphaltene (PAA) solid fraction from the liquid product yield, it was found that the yield of PAAs increased with rising reaction temperature (Figure 1). Notably,

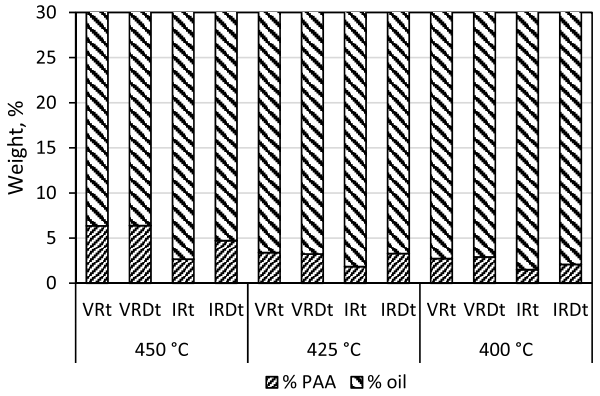


Figure 1. Preasphaltene and asphaltene yields from liquid products produced from tetralin liquefaction at 400−450 °C.

the PAA yield from the VR and VRD experiments remained relatively consistent, implying that ash constituents do not exert a significant influence during the catalytic breakdown of PAA molecules. In contrast, the IR PAA yields were lower compared to the PAAs from IRD liquefaction at all reaction temperatures. A lower hydrogen content in the IRD feed could result in products that are more aromatic in nature, supported by a lower H/C ratio of the solid and liquid yield. Another potential explanation could be that the inorganic minerals present in the IR coal act as catalysts for the decomposition of larger molecules, which typically result in the production of PAA. Alternatively, it is plausible that inorganic minerals inhibit recombination reactions that lead to the formation of PAA molecules. The IR liquefaction yields exhibited the lowest PAA yield across all temperature ranges. Asphaltenes are formally defined as materials insoluble in alkanes (such as *n*-pentane, *n*-hexane, and *n*-heptane) but soluble in aromatics such as benzene and toluene. Due to their bulky nature, they can be regarded as the nonpolar and nonvolatile components in crude oil.[33] However, the extraction efficacy becomes apparent at higher temperatures (e.g., 85 °C) due to the potential precipitation of polar compounds at lower temperatures, which might incorrectly contribute to the calculated PAA yield.

3.2. Characterization of Solid Fractions Obtained during Liquefaction Experiments. *3.2.1. Physicochemical and Structural Characterization.* Table 4 shows the approximated proximate analysis and calorific values of solid residues produced from tetralin liquefaction at 450 °C. The volatile matter contents within the liquefaction solid residues are comparatively lower, while the fixed carbon contents are higher compared to the original coal samples, and this observation becomes more pronounced as the liquefaction temperatures are increased (as shown in Tables 1, 4, and S1). Nonetheless, when considering a dry ash-free basis, the carbon

https://doi.org/10.1021/acsomega.4c00602
ACS Omega 2024, 9, 12272−12289

Table 4. Approximated Proximate Analysis, Calorific Values, and Ultimate Analysis of Solid Residues Produced from Tetralin Liquefaction at 450 °C[a]

sample identification	VR SR	VR PAA	VRD SR	VRD PAA	IR SR	IR PAA	IRD SR	IRD PAA
% moisture content	1.5	3.6	2.7	3.7	0.8	3.1	1.9	4.5
% ash yield	45.1	0.8	2.0	1.0	48.3	3.0	3.0	0.1
% volatile matter	11.3	38.0	13.1	38.5	14.1	31.1	11.8	37.9
% fixed carbon (by calculation)	42.1	57.7	82.1	56.8	36.7	62.8	83.3	57.6
fuel ratio	3.7	1.5	6.3	1.5	2.6	2.0	7.1	1.5
calorific values (MJ kg^{-1})	17.0	-	33.6	-	15.9	-	33.6	-
HHV (MJ kg^{-1}) (eq 5)	16.5	27.3	31.9	27.1	14.9	27.9	31.9	27.5
% carbon content	82.0	-	87.4	-	82.9	-	88.5	-
% hydrogen content	3.6	-	3.8	-	3.8	-	3.7	-
% nitrogen content	2.6	-	2.4	-	2.2	-	2.0	-
% oxygen content (calculated)	10.8	-	5.9	-	9.4	-	5.0	-
% total sulfur	1.0	-	0.5	-	1.7	-	0.8	-
O/C molar ratio	0.10	-	0.05	-	0.08	-	0.04	-
H/C molar ratio	0.52	-	0.52	-	0.54	-	0.49	-

[a]Approximated from thermogravimetric analysis. SR = Liquefaction solid residue; PAA = preasphaltenes and asphaltenes.

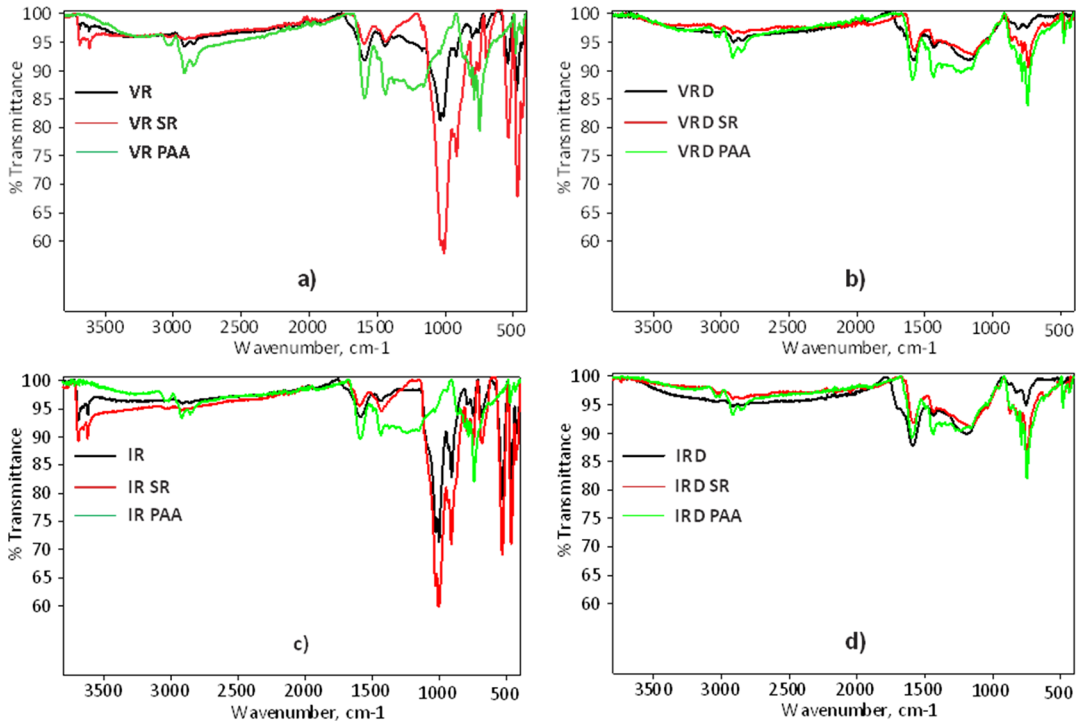


Figure 2. Infrared spectra of the solid feed materials, including solid residues and PAAs produced from tetralin liquefaction at 450 °C from (a) VR coal, (b) VRD coal, (c) IR coal, and (d) IRD coal.

and hydrogen contents of the residues exhibit only a minor increase compared to the original coal. Additionally, a significant portion of these residues can be transformed into syngas (CO and H_2) during the gasification process and further utilized in DCL plants.[14] The low calorific values or HHVs of the VR- and IR-derived solid residues are a result of the high ash yields in the samples. Compared to the higher heating values of the solid liquefaction residues of the demineralized coal and residue samples, the HHVs of the residues increase as the liquefaction temperature rises. The proximate analysis and higher heating value results for the liquefaction experiments conducted at 425 and 400 °C in tetralin and 450 °C in benzene are presented in Table S1.

Inertinites usually contain higher proportions of elemental carbon and lower proportions of elemental hydrogen compared to vitrinites and liptinites. Within this maceral group, fusinites and semifusinites also show fossilized woody structures, but contain less hydrogen and more carbon than vitrinites.[34] Comparing the O/C and H/C molar ratio from Tables 1 and 4, it is clear that the residues produced from the liquefaction experiments had notably lower O/C and H/C values than their respective feed materials. This leads to the assumption that more aliphatic and polar structures reacted during liquefaction experiments.[10,27] H/C molar ratios decreased more in the residues produced from VR liquefaction compared to IR. This is consistent with literature indicating that H/C values and aromaticity for principle maceral groups decrease during pyrolysis and liquefaction processes in the order: liptinite > vitrinite > inertinite.[34] Gasification reactivities of these solid residue chars are expected to be relatively lower

https://doi.org/10.1021/acsomega.4c00602
ACS Omega 2024, 9, 12272−12289

during CO_2 gasification, while higher activation energies (E_a) are required when compared to the raw feed materials (discussed in Section 3.2.3).

Figure 2 shows the IR spectra of the VR (a), VRD (b), IR (c), and IRD (d) coals; and their respective solid residues (SR) and preasphaltenes and asphaltenes (PAA) produced from tetralin liquefaction conducted at 450 °C. No strong O−H stretching vibrations from intermolecular hydrogen bonding are observed in the 3400−3200 cm^{-1} regions for all raw, SR, and PAA samples (Figure 2a−d). However, strong O−H stretching vibrations of nonhydrogen-bonded or "free" hydroxyl groups of alcohols and phenols absorb strongly in the 3700−3584 cm^{-1} region and can only be observed in the VR, VR SR, IR, and IR SR fractions.[35] No absorption peaks in these regions were observed in the PAAs produced from the liquefaction of the VR and IR coals. Meanwhile, no hydroxy bands were observed in the spectra of the demineralized materials and their respective solid residues and PAAs. The acid treatment (with HCl and HF) during demineralization may promote the reaction between H-X acids and alcohols to form alkyl halides (and H_2O, which is mostly removed during drying).[16] It is also evident that no polar structures containing −C═O and −OH functional groups were removed from the liquid residues during the PAA separation process. This can be supported by absent C═O stretching and O−H stretching bands in the 1750−1650 cm^{-1} and 3700−3200 cm^{-1} regions of the PAAs. The intensities of aliphatic sp^3 C−H stretching bands at 2915−2840 cm^{-1} of the solid residues (SRs) are weaker than the corresponding signals of the coal samples (VR, VRD, IR, and IRD), while no distinctive bands are observed in the spectra of the PAAs. From Figure 2a,c, it follows that strong aromatic C═C stretching vibrations are observed near 1592 cm^{-1} and their intensities decrease in order: PAA > Raw > SR for the VR and IR fractions. The IR bands from VR, VRD, IR, and IRD in this region overlap with weak C═O stretching bands of carbonyl groups such as aldehydes, ketones, and esters in the 1960−1700 cm^{-1} region. The solid residues and PAAs appear to have no C═O stretching bands in this region.

It can be deduced that more aliphatic components decompose to produce liquids and gases and that the solid residues derived from the coals and demineralized coals were more aromatic in nature. Weak aromatic sp^2 C−H bands in the 3200−3000 cm^{-1} region indicate that macromolecular structures of the feed materials and solid residues are mostly made up of quaternary aromatic carbons, while the PAAs have bands in this area accounting for more C−H bonds. It can also be established that the PAAs have more aliphatic components because of stronger sp^3 C−H stretching bands in the 3000−2850 cm^{-1} region. The peak intensities of acyl and alkoxy C−O stretching bands at 1200−1000 cm^{-1} of the VR and IR coals are weaker than their respective SRs but have stronger aromatic C═O stretching bands near 1586 cm^{-1}. The results indicate that acyl and alkoxy C−O groups are less reactive during liquefaction experiments than carbonyl (C═O) groups; this includes cleavage of C−O-R linkages. No significant differences in this region were observed for the demineralized materials and their respective SRs and PAAs. These findings suggest that the organic structure of the coals was modified during the acid treatment process, as has been investigated by others.[16]

3.2.2. X-ray Diffraction and CO_2 Low-Pressure Adsorption Analysis. The XRD results revealed that the demineralized samples (VRD and IRD) and their respective residue samples contained significantly high (>98%) amorphous materials, while the PAA samples contained 100% amorphous materials—predominantly consisting of organic carbons.[13] These results were not reported in this work. Table 5 shows the XRD analysis results of the VR and IR samples with their respective solid residue products produced via tetralin liquefaction at 450 °C. The samples contained high amounts of amorphous phases with some crystalline phases. The XRD results reveal that the most abundant crystalline minerals in the samples are quartz (SiO_2) and clay minerals like kaolinite ($Al_2Si_2O_5(OH)_4$) with minor amounts of dolomite, calcite, muscovite, and magnetite. The IR coal sample has a higher fraction of kaolinite compared to the VR coal sample. The decomposition of kaolinite (to meta kaolinite) generally occurs at around 450 °C[13,19]; however, no changes in the diffractograms were observed that suggest the presence of meta kaolinite in the residue samples (VR SR and IR SR). It should also be noted that kaolinite and smectite peaks overlap and further tests would be necessary to distinguish between these.

Table 5. Relative Mineral Phase Amounts (wt %) of the Coals and Their Solid Residues Produced at 450 °C during Tetralin Liquefaction

mineral phases (%)	VR	VR SR	IR	IR SR
quartz	7.5	13.8	7.7	11.6
kaolinite	11.0	18.0	28.8	28.0
dolomite	-	0.1	4.4	4.7
calcite	-	<0.1	1.0	0.6
muscovite	1.0	1.2	3.1	2.7
magnetite	-	<0.1	0.5	0.6
smectite	2.8	-	-	-
pyrrhotite	-	<0.1	-	0.3
sepiolite	-	12.8	-	-
amorphous/organic carbon	77.7	54.0	54.4	51.4

The behavior of minerals during liquefaction depends on the specific mineral, the conditions of the liquefaction process, and the duration of exposure to high temperatures and pressures. The results, however, indicate that most minerals from the IR coal did not undergo major structural changes and remained stable under these liquefaction conditions.

Different structural parameters were calculated by fitting XRD patterns obtained from the different samples. The values of d_{002} (interlayer spacing), L_c (stacking height of graphitic planes), L_a (crystallite size), and n (degree of crystallinity) are presented in Table 6. These results provide insight into the structural changes that occur during coal liquefaction and are indicative of the coal's crystalline structure, degree of graphitization, and overall maturity. These changes are highlighted by comparing the properties of the original feed materials (VR, VRD, IR, and IRD), the solid residues chars (VR SR, VRD SR, IR SR, and IRD SR), and the preasphaltenes/asphaltenes (PAA) obtained from the liquid fraction of the liquefaction experiments.

The d_{002} parameter reflects the interlayer spacing within the coal structure. It is noticeable that this parameter decreases in the solid char residues (VR SR, VRD SR, IR SR, and IRD SR) compared to the feed materials (VR, VRD, IR, and IRD). The d_{002} values decrease from 3.74 Å in VR to 3.53 Å in VR SR and from 3.61 Å in VRD to 3.42 Å in VRD SR, while IR SR and IRD SR also show decreases in d_{002} compared to their parent

https://doi.org/10.1021/acsomega.4c00602
ACS Omega 2024, 9, 12272−12289

Table 6. Structural Parameters Obtained by Fitting XRD Patterns from the Feed Materials, Solid Residues, and PAA

sample	d_{002} (Å)	L_c (Å)	L_a (Å)	n
VR	3.74	8.69	-	3.33
VR SR	3.53	11.06	-	4.13
VR PAA	3.49	19.52	26.46	6.60
VRD	3.61	15.21	53.37	5.22
VRD SR	3.42	42.36	34.91	13.38
VRD PAA	3.49	16.46	29.81	5.72
IR	3.67	12.23	-	4.33
IR SR	3.66	12.41	-	4.39
IR PAA	3.47	20.91	28.71	7.02
IRD	3.46	20.61	47.73	6.96
IRD SR	3.44	43.45	-	13.64
IRD PAA	3.49	20.84	41.53	6.98

coals. This decrease suggests a compaction and reduction in the interlayer spacing during coal liquefaction, and that the coal's crystalline structure becomes more ordered and compact as a result of the liquefaction process. Such compaction is often associated with the removal of volatile matter and the rearrangement of carbon atoms, leading to higher carbon content and increased maturity. Demineralization significantly affects the coal structure, as indicated by the larger d_{002} values in demineralized samples (VRD and IRD) compared to their parent coals (VR and IR), suggesting an expansion of the crystalline structure due to the removal of mineral impurities. The crystallite size (L_c) of inertinite is larger than that of vitrinite macerals in coals.[36] These values generally increase in liquefaction solid residues, reflecting the growth of crystallites and the stacking height of graphitic planes, and are indicative of a higher degree of graphitization during liquefaction. The results are consistent with the literature.[7,26] The L_a parameter represents the crystallite size within the coal structure. The results show that the crystallite size (L_a) tends to increase in the solid char residues compared to the feed materials. This increase in crystallite size indicates that the coal's macromolecular structure becomes more ordered and extended during liquefaction. Larger crystallites are associated with higher degrees of crystallinity and increased graphitization, which is a sign of enhanced structural maturity. Similar results were found by other authors.[7,26]

The solid char residues (SR) reflect the structural compaction and enhanced graphitization (and recombination reactions) that occur during liquefaction, while the PAA fractions demonstrate the retention of structural order and crystallinity in the soluble components formed during the process. Furthermore, during coal maturation, molecular chains reconnect into larger macromolecular chains, leading to increased maturity and aromaticity in both VR and IR. The shedding of aliphatic side chains and oxygen functional groups results in a more orderly arrangement of coal macromolecules, leading to fewer lattice defects in carbon atoms and a structure closer to graphitization, which shows the decrease of d_{002} and the increase of L_a and L_c. These structural changes may influence the gasification reactivities of the samples by affecting the accessibility of reactive sites and the overall reactivity of the carbonaceous material.

Table 7 presents the CO_2 low-pressure adsorption analysis results of the coal samples, their solid residues, and PAAs. It appears that the liquefaction process generally reduces the surface area. For example, VR has a higher BET surface area

Table 7. CO_2 Low-Pressure Adsorption Analysis of the Coal and Demineralized Coal Samples and Their Respective Liquefaction Solid Residues and PAAs Produced at 450 °C[a]

sample	BET surface area, m^2/g	D−R micropore surface area, m^2/g	H−K pore volume, cm^3/g (×10^2)	H−K median pore width, Å
VR	90.1	112.5	3.55	3.84
VR SR	42.6	55.0	1.61	3.95
VR PAA	1.9	15.2	0.18	4.67
VRD	96.7	120.1	3.80	3.84
VRD SR	59.3	66.8	1.86	4.03
VRD PAA	1.3	16.2	0.17	4.69
IR	69.5	85.8	2.76	3.80
IR SR	32.6	41.9	1.15	4.02
IR PAA	2.1	18.7	0.24	4.63
IRD	93.4	116.2	3.81	3.77
IRD SR	55.2	62.7	1.67	4.09
IRD PAA	1.4	16.5	0.15	4.70

[a]BET = Brunauer−Emmet−Teller; D−R = Dubinin−Radushkevich; H−K = Horvath−Kawazoe.

(90.1 m^2/g) compared to VR SR (42.6 m^2/g). Similarly, IR has a higher BET surface area (36.5 m^2/g) compared to IR SR (32.6 m^2/g), suggesting a decrease in the surface area after liquefaction. Similar to the BET surface areas, the D−R micropore surface areas tend to decrease in the solid residues compared to the parent coal samples after liquefaction. For example, VR has a higher D−R micropore surface area (112.5 m^2/g) compared to VR SR (55.0 m^2/g), indicating a reduction in the micropore surface area. Similarly, IR has a higher D-R micropore surface area (85.8 m^2/g) compared to IR SR (41.9 m^2/g). In addition, the liquefaction process generally leads to a decrease in pore volume in the solid residues compared to the parent coal samples. For instance, VR has a higher H−K pore volume (3.55 $cm^3/g \times 10^2$) compared to VR SR (1.61 $cm^3/g \times 10^2$), indicating a reduction in pore volume after liquefaction. Similarly, IR has a higher H−K pore volume (2.76 $cm^3/g \times 10^2$) compared to IR SR (1.15 $cm^3/g \times 10^2$), suggesting a decrease in pore volume due to liquefaction. VRD and IRD also follow these trends. The median pore width values appear to increase slightly from the parent coal samples to their solid residues.

Coal liquefaction tends to reduce the surface area, micropore surface area, and pore volume of the solid residues compared to the parent coal samples. This suggests that the liquefaction process results in a reduction in porosity and available surface area for gasification reactions in the solid residues. Consequently, the solid residues from coal liquefaction may exhibit lower gasification reactivities compared to the original coal samples, primarily due to the alteration of their porous structure during the liquefaction process. These changes encompass the breakage of carbon−carbon bonds, the removal of specific functional groups, and the consequent widening of the existing pores. Moreover, these reactions may lead to the loss of micropores, resulting in an increase in the average pore size. Additionally, smaller pores have the propensity to coalesce or merge into larger ones during conversion, ultimately contributing to an overall expansion in average pore width.

3.2.3. Thermogravimetric Analysis: Pyrolysis, CO_2 Gasification, and Kinetics. Figure 3 illustrates a standard

https://doi.org/10.1021/acsomega.4c00602
ACS Omega 2024, 9, 12272−12289

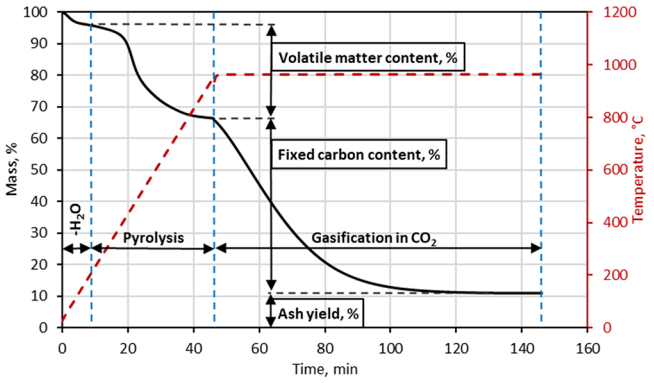


Figure 3. Thermogravimetric analysis: Mass loss profile during pyrolysis under N_2 and isothermal CO_2 gasification.

thermogravimetric analysis graph for coal, detailing its behavior during pyrolysis and CO_2 gasification. This curve can be divided into three distinct phases: the dewatering stage below 180 °C, the pyrolysis stage in a nitrogen (N_2) atmosphere from 180−960 °C, and the isothermal gasification stage at 960 °C.

In Figure 4a−d, pyrolysis curves are presented for the following coal samples: (a) VR, (b) VRD, (c) IR, and (d) IRD. These curves also depict the amounts of solid residues and PAAs obtained during liquefaction experiments conducted at 450 °C, utilizing tetralin as the solvent.

Table 8 presents results from the CO_2 gasification experiments at 960 °C on the vitrinite-rich (VR) and inertinite-rich (IR) coals, their demineralized variants (VRD and IRD), as well as the solid char residues (VRSR, VRDSR, IRSR, and IRDSR) and the PAA (asphaltenes and preasphaltenes) removed from liquid fractions obtained from liquefaction experiments at 450 °C in tetralin. Various parameters, such as $t_{0.5}$ (time for 50% conversion), $R_{0.5}$ (reactivity at 50% conversion), $t_{0.9}$ (time for 90% conversion), $R_{0.9}$ (reactivity at 90% conversion), R_i (initial reactivity), and R_{fa} (average final reactivity) for CO_2 gasification, have been determined.

VR SR, VRD SR, and IRD SR chars exhibit higher reactivities at 50% conversion ($R_{0.5}$) compared to their parent coal chars, i.e., VR, VRD, and IRD. This indicates that the liquefaction process produces char residues with enhanced gasification reactivities. This trend did not hold for the IR SR char and its parent coal (IR) char. The VRD (demineralized VR) char exhibits lower $R_{0.5}$ values compared to VR char, while similar results were obtained for the IRD (demineralized IR) and IR chars. VRD and IRD chars display lower initial reactivities (R_i) compared to the VR and IR chars. In this context, the presence of inorganic minerals appears to have a

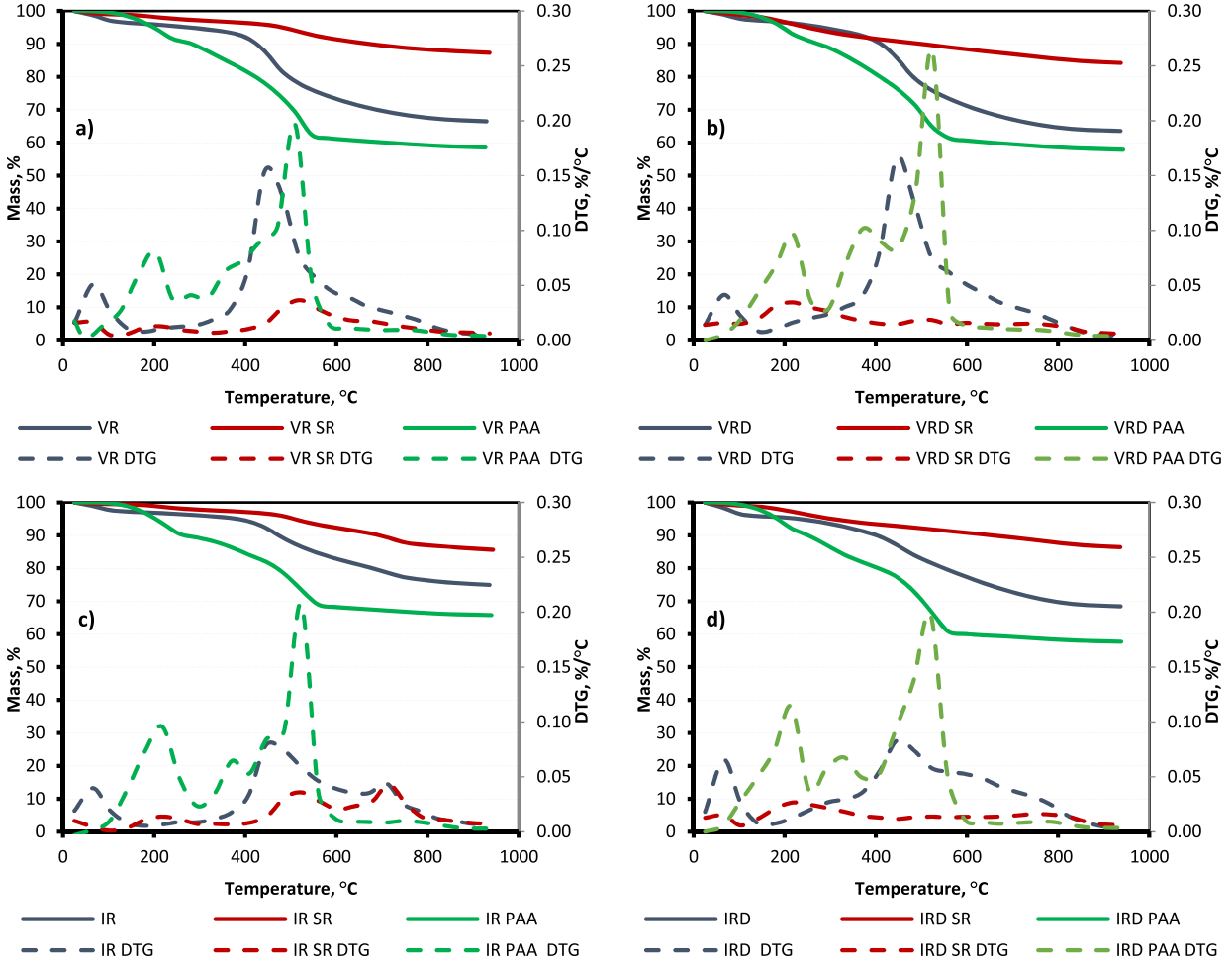


Figure 4. Pyrolysis curves are presented for the following coal samples: (a) VR, (b) VRD, (c) IR, and (d) IRD, with their respective solid residues and PAAs obtained during liquefaction experiments conducted at 450 °C, utilizing tetralin as the solvent.

https://doi.org/10.1021/acsomega.4c00602
ACS Omega 2024, 9, 12272−12289

Table 8. CO_2 Gasification Reactivities at 960 °C of the Coal and Demineralized Coal Samples and Their Respective Solid Residues and PAAs Produced from Tetralin Liquefaction at 450 °C[a]

		VR			VRD			IR			IRD		
reactivities		raw	SR	PAA	raw	SR	PAA	raw	SR	PAA	raw	SR	PAA
$t_{0.5}$, min		18.3	12.9	408.1	28.8	15.6	335.0	14.5	20.9	291.3	14.6	11.3	243.1
$t_{0.9}$, min		41.3	44.4	814.7	52.8	44.3	631.2	40.1	69.2	605.2	28.5	23.5	508.0
$R_{0.5}$, min^{-1}	$\times 10^2$	2.73	3.88	0.12	1.74	3.21	0.15	3.44	2.39	0.17	3.42	4.43	0.21
$R_{0.9}$, min^{-1}	$\times 10^2$	2.18	2.03	0.11	1.71	2.03	0.14	2.24	1.30	0.15	3.16	3.84	0.18
R_i, min^{-1}	$\times 10^2$	2.29	4.92	0.12	1.21	2.86	0.14	4.38	3.77	0.24	2.71	3.21	0.24
R_{fa}, min^{-1}	$\times 10^2$	1.37	0.89	0.09	1.43	1.09	0.12	1.22	0.65	0.11	2.43	2.65	0.13

[a]Raw—feed materials; SR—solid residues; PAA—preasphaltene and asphaltene.

catalytic effect on the initial carbon conversion reactions and the removal of inorganic minerals through demineralization can inhibit gasification reactions.[37]

Furthermore, a more pronounced catalytic effect can be observed on the initial carbon conversion of the IR coal, characterized by a higher ash yield, when compared to the VR coal. A higher R_i value indicates a higher initial reactivity, meaning that the char is more reactive at the beginning of the reaction than at 50 and 90% conversion. Nevertheless, this phenomenon was not evident for the demineralized materials, where the initial reactivities were lower than the reactivities observed at 50 and 90% conversion. Sakawa et al.[37] found that CO_2 gasification rates were higher in coals with higher inertinite contents but also expressed that higher inertinite contents were generally accompanied by high alkali indices.[38]

However, the catalytic effect of inorganic minerals in the IR coal appears to outweigh the inherently lower reactivity of inertinite-rich macerals, leading to a higher R_i in the IR coal. The data indicate that, despite the inherently higher reactivity of vitrinite-rich macerals in VR coal, the higher ash yield and the catalytic effect of inorganic minerals in IR coal result in a more pronounced increase in initial reactivity (R_i) in the IR coal. This suggests that the catalytic effect of inorganic minerals can be particularly influential in enhancing the initial stages of carbon conversion reactions during gasification.[38] Lower L_c values of chars, indicative of smaller crystallite sizes and stacking height of graphitic planes, generally suggest that the accessibility of active sites is enhanced, resulting in higher reactivities during gasification, whereas larger crystallite sizes are not favored during gasification.[32,36] When comparing the L_c values of VR SR (11.1 Å) and IR SR (12.4 Å), lower overall reactivities of the IR SR char were observed. However, the reactivities of the solid residue chars obtained from the demineralized coal samples do not correlate with this trend, where R_i, $R_{0.5}$, $R_{0.9}$, and R_{fa} of IRD SR (l_c = 43.5 Å) are significantly higher than VRD SR (L_c = 42.3 Å). These results can be supported by the inhibiting or hindering effects of mineral matter in the IR coal sample and solid residue.[31,32,37] This hindering effect can particularly be observed at the end of conversion—highlighted by lower R_{fa} values during char gasification reactions of the IR compared to the VR coals.

The gasification reactivity of coal generally decreases as the carbon content increases, corresponding to higher coal maturity. Various factors contribute to the variations in gasification reactivity, including the influence of pyrolysis conditions on the distinct mineral matter contents of the coals. Several char properties crucial for gasification, like surface area, porosity, chemical composition, and active site presence, are altered during pyrolysis and are influenced by the initial coal properties. The initial characteristics of the coal are thus unavoidably influenced by the chemical and physical processes that occur during the intermediate pyrolysis stage. In fact, the findings indicate that the pyrolysis step primarily determines the gasification reactivity of the char materials.[34] The mass loss curves from the CO_2 gasification experiments of the VR, VRD, IR, and IRD coal samples and their respective liquefaction solid residues (produced at 450 °C) at 900, 930, and 960 °C are presented in Figure S2.

Table S2 shows the CO_2 gasification reactivities of solid residues produced from tetralin liquefaction at 425 and 400 °C and benzene liquefaction at 450 °C. From these results, the initial reactivities, R_i, of the liquefaction residue chars were mainly affected by liquefaction temperature. While the R_i of the residues derived from the VR coal increased at higher temperatures, i.e., the R_i of the residues derived from the IR coal decreased at higher liquefaction temperatures. Notably, the VRD solid residues and IRD solid residues showed the highest R_i values at 425 °C.

Proximate analysis results indicate that a higher fraction of fixed carbon content is achieved at higher liquefaction temperatures (Tables 4 and S1). Similarly, the fuel ratios of the liquefaction residues increased, indicating that volatile hydrocarbons are more prone to react during the liquefaction process. In general, vitrinite macerals contain a higher fraction of volatile matter compared to inertinite macerals because inertinite macerals have undergone a more advanced stage of coalification. This means that a larger portion of inertinite is composed of solid, carbonaceous material with a higher fixed carbon content compared to vitrinite macerals.[34]

The random pore model (RPM) and the volumetric reactive model (VRM) were applied to the obtained CO_2 gasification results to determine parameters such as time factors (t_f) and structural parameters (Ψ) using eqs 24 and 28, respectively. The accuracy of the two models was assessed using uncertainty parameters. These parameters, namely, the quality of fit (QOF), determined from eq 27, and the error sum of square (ESS), were derived from the model fitting process. The summary of the RPM- and VRM-derived time factors (t_f), structural parameters (Ψ), quality of fit (QOF), and error sum square (ESS) at different temperatures for the VR and IR coals, as well as their respective solid residue chars and PAAs, is presented in Table S3. QOF values obtained from the RPM varied from 98.9 to 99.8 for the VR coal chars and 98.1 to 99.7 for the IR coal chars. Lower values were obtained using the VRM. The RPM considers a pore structure characterized by random overlap, resulting in a reduction in the available reaction area. This model can predict the maximum reactivity value as the reaction progresses because it simultaneously considers the effects of pore growth during the initial

https://doi.org/10.1021/acsomega.4c00602
ACS Omega 2024, 9, 12272−12289

Table 9. Apparent Activation Energies (E_a, kJ mol^{-1}) and Lumped Pre-Exponential Factors (k_{SO}, min^{-1}) Calculated using the Different Reaction Reactivity Models from CO_2 Gasification Experiments of VR and IR, and Their Respective Solid Residue Fractions Produced from Tetralin Liquefaction at 450 °C[a]

sample	reactivity model	R^2	slope	intercept	E_a (kJ mol^{-1})	k_{SO} (min^{-1})
VR	R_i	0.985	−21203.9	13.38	176.3	6.5×10^{05}
	$R_{t0.5}$	1.000	−24220.8	16.04	201.4	9.2×10^{06}
	$t_{f(RPM)}$	0.992	−22174.8	14.16	184.4	1.4×10^{06}
	$t_{f(VRM)}$	1.000	−24280.4	16.58	201.9	1.6×10^{07}
	R_{fa}	1.000	−24374.8	15.48	202.7	5.3×10^{06}
VR SR	R_i	0.952	−20524.1	13.69	170.6	8.8×10^{05}
	$R_{t0.5}$	0.982	−27809.7	19.35	231.2	2.5×10^{08}
	$t_{f(RPM)}$	0.986	−28282.3	20.04	235.1	5.1×10^{08}
	$t_{f(VRM)}$	0.986	−28281.5	20.04	235.1	5.1×10^{08}
	R_{fa}	0.998	−27138.4	17.30	225.6	3.3×10^{07}
IR	R_i	0.998	−13044.8	7.46	108.5	1.7×10^{03}
	$R_{t0.5}$	0.999	−22582.9	14.95	187.8	3.1×10^{06}
	$t_{f(RPM)}$	0.996	−20712.7	13.66	172.2	8.6×10^{05}
	$t_{f(VRM)}$	0.999	−23729.3	16.30	197.3	1.2×10^{07}
	R_{fa}	1.000	−26385.1	16.99	219.4	2.4×10^{07}
IR SR	R_i	0.978	−13282.3	7.52	110.4	1.8×10^{03}
	$R_{t0.5}$	0.999	−20688.5	13.05	172.0	4.7×10^{05}
	$t_{f(RPM)}$	0.999	−20047.0	12.84	166.7	3.8×10^{05}
	$t_{f(VRM)}$	0.999	−20097.7	12.88	167.1	3.9×10^{05}
	R_{fa}	0.999	−23737.3	14.21	197.4	1.5×10^{06}

[a]The natural logarithm of R_i, $R_{t0.5}$, and R_{fa} were plotted against $1/T$ (K^{-1}) to approximate the values for E_a and k_{SO}.

gasification stages and the destruction of pores due to the coalescence of adjacent pores.[39]

The structural parameters, Ψ, of the VR chars were found to increase from 4.9 to 6.5 with increasing isothermal temperature (900−960 °C). Similarly, the structural parameters of the IR chars increased with isothermal temperature, ranging from 0.23 to 0.77. The structural parameters obtained from the VR coal char indicate that pore growth occurred during the early stages of the gasification process (Ψ > 2) and that increased surface areas are expected during further carbon conversion, whereas the values from the IR coal char indicate that pore coalescence was favored during the early stages of the gasification process (Ψ < 2), and surface areas are expected to decrease during further carbon conversion. As expected, the time factors, t_f, obtained from the coal chars and their liquefaction residue chars increased with increasing isothermal temperature. Similar results on South African bituminous coals were observed by other researchers.[13,26,40] Structural parameters of the VR SR and IR SR chars were found to be 0.00 at all isothermal temperatures, which implies that both the random pore model and volumetric reaction model can be used to estimate the apparent activation energies of the chars during gasification (QOF values were the same for these materials). In addition, pore coalescence is expected to be mostly favored during the early stages of gasification. The VRM implies that chemical reactions take place simultaneously at all sites within the particle and the reaction surface linearly decreases with increasing char conversion.[39] This is supported by the lower average final reactivities obtained from the CO_2 gasification of the liquefaction solid residue chars, as presented in Table 8.

The E_a values estimated from the gasification reactions of all PAAs were difficult to calculate and values obtained from the different reactivity parameters and t_f values were inconsistent (Table S3). R^2 values derived from the reactivities at different isothermal temperatures were also low. This can be a result of significantly low gasification reactivities where model fitting becomes difficult. From Table S3, the structural parameters, Ψ, of the PAA chars were expected to be higher compared to their parent coal-derived chars, and as per definition, larger structural parameters are indicated by low surface areas and smaller porosities.[12] This was true for the gasification reactions at 960 °C for the IR coal char (Ψ = 0.77; BET = 69.5 m^2/g) and IR PAA (Ψ = 7.59; BET = 2.1 m^2/g) and for the VR coal char (Ψ = 6.47; BET = 90.1 m^2/g) and VR PAA (Ψ = 17.39; BET = 1.9 m^2/g). The structural parameters obtained from the VR and VRD coal chars and their respective PAAs were found to be inconsistent with this trend at gasification reactions conducted at 900 and 930 °C.

Using the values of R_i, $R_{0.5}$, R_{fa}, t_f (RPM), and t_f (VRM) from the char CO_2 gasification results of VR, VR SR, IR, and IR SR, Arrhenius plots were constructed to estimate the apparent activation energies (E_a, kJ mol^{-1}) and lumped pre-exponential factors (k_{SO}, min^{-1}) from eq 26. These results are presented in Table 9. The results from the demineralized coals and their liquefaction residue chars and PAAs are summarized in Table S4.

Estimated from the random pore model, the apparent activation energies of the gasification reaction were 184.4 kJ mol^{-1} for the VR char, 235.1 kJ mol^{-1} for the VR SR char, 172.2 kJ mol^{-1} for the IR char, and 166.7 kJ mol^{-1} for the IR SR char. The E_a values obtained from the char gasification reactions indicate lower overall apparent activation energies for the IR coal compared to the VR coal. However, a higher E_a was obtained for IR using R_{fa} parameters, indicating that more energy is needed to convert the char fraction between $X = 0.7$ and 0.9. These values are inversely proportional to the char CO_2 gasification reactivities obtained from the IR and VR coal samples. Other researchers have established that chars with a higher gasification reactivity usually have lower apparent activation energies.[13,26] However, the reported E_a estimated from all parameters of the solid residue chars indicate that IR SR char had significantly lower E_a values (accompanied by

https://doi.org/10.1021/acsomega.4c00602
ACS Omega 2024, 9, 12272−12289

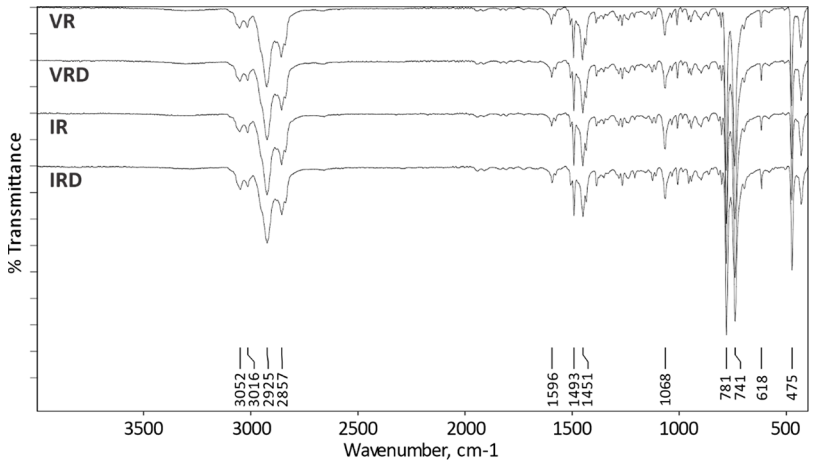


Figure 5. FTIR spectra of liquid/oil residues obtained from tetralin liquefaction conducted at 450 °C on the VR, VRD, IR, and IRD coals.

lower gasification reactivity) compared to VR SR char, but comparable values to the IR char.

3.3. Characterization of Liquid Yields from Liquefaction Experiments. *3.3.1. FTIR Spectroscopy of Liquid Yields.* The FTIR spectra of the liquid/oil products produced from tetralin liquefaction of VR, VRD, IR, and IRD coals at 450 °C are presented in Figure 5. Preasphaltenes/asphaltenes (PAAs) were removed prior to FTIR spectroscopic analysis. The FTIR spectra of the liquid products from benzene liquefaction are presented in Figure S4. The FTIR spectra of the two solvents used, namely, tetralin and benzene, are presented in Figure S5.

Relevant FTIR wavenumbers (cm^{-1}): 3052 and 3016 (sp^2 C−H stretch, aromatic); 2925 and 2857 (sp^3 C−H stretch, methylene/CH_2); 1596, 1493, and 1451 (C═C stretch, aromatic); 1068 (C−O stretch, alkoxy); 781 and 741 (out-of-plane sp^2 C−H bend, ortho disubstituted aromatics); 618 (sp^2 C−H bend, methylene/CH_2); 475 (out-of-plane ring bending).

Aromatic sp^2 C−H bands in the 3200−3000 cm^{-1} region indicate that the molecular structures of the liquid residues are similar to that of tetralin, signifying aromatic structures with connected methylene groups (methylene C−H stretch, 2925 and 2857 cm^{-1}). Bands with slightly higher intensities at 1596 cm^{-1} indicate more aromatic C═C groups are present in the liquid products and signify the formation of naphthalene during liquefaction. This can be supported by a strong out-of-plane sp^2 C−H bending vibration for ortho disubstituted aromatics at 781 cm^{-1}.[35] The band at 741 cm^{-1} indicates that a notable amount of unreacted tetralin is present. The results can be supported by the GC-MS results presented in Table 10. Evidently, no polar structures containing −C═O and −OH functional groups were produced from the coal samples during the liquefaction process. This can be supported by absent C═O stretching and O−H stretching vibrations in the 1750−1650 and 3700−3200 cm^{-1} regions. Meanwhile, weak alkoxy C−O stretching vibrations at 1068 cm^{-1} are observed in the liquid products.

From Figure S4, presenting the FTIR spectra of the liquid fractions derived from benzene liquefaction conducted at 450 °C, aromatic sp^2 C−H stretching bands can be observed in the 3200−3000 cm^{-1} range with no evidence of sp^3 C−H stretching bands in the 2950−2800 cm^{-1} region. This signifies that aromatic structures (like benzenes) are present without any detectable methylene groups (sp^3 C−H). However, from mass balance calculations, a fraction of hydrogen from the feed materials was transferred to the liquid fraction, most likely through hydrogenation reactions. It is possible that the large fraction of unreacted benzene present, supported by the low conversion values from benzene liquefaction, may suppress these methylene bands. The bands observed at 1715 and 1266 cm^{-1} can be assigned to C═O stretching and acyl C−O stretching bands, respectively. The C═O stretching band is in the region for benzoate esters, i.e., 1730−1715 cm^{-1}. Similar to the liquid yields from tetralin liquefaction, bands of out-of-plane sp^2 C−H bending vibrations of substituted aromatics are observed at 738 cm^{-1}.

Table 10. Approximate Ultimate Analysis and Calorific Values of Liquid Yields from Tetralin Liquefaction at 450 °C[a]

sample identification	tetralin	VR_{liq}	VRD_{liq}	IR_{liq}	IRD_{liq}
% carbon content	90.85	86.9	85.9	87.3	85.7
% hydrogen content	9.15	7.9	7.8	8.1	7.7
% nitrogen content	n.d.	2.9	3.7	2.8	4.0
% oxygen content (calculated)	n.d.	2.2	2.7	1.7	2.5
% total sulfur	n.d.	0.1	0.0	0.1	0.0
O/C molar ratio	0.00	0.02	0.02	0.01	0.02
H/C molar ratio	1.20	1.08	1.07	1.11	1.07
calorific values (MJ kg^{-1})	42.4	42.3	42.8	42.1	42.1

[a]Feed materials—VR, VRD, IR, and IRD; liq−liquid yield; n.d. − not determined.

No distinctive differences between the spectra of the VR, VRD, IR, and IRD liquid residues derived from tetralin liquefaction were observed. The same conclusion can be made for the liquid residues derived from benzene liquefaction, indicating that the liquefaction process produces compounds with similar structural characteristics.

3.3.2. Ultimate Analysis, Calorific Values, and GC-MS of Liquid Yields. Through mass balance calculations, presented in Table S5, the approximate ultimate analysis values of the liquid yields from tetralin liquefaction at 450 °C were determined, as presented in Table 10. When considering Table 1, it is evident that the low hydrogen content of the coal samples affected the final hydrogen content of the liquid yields. The lower H/C molar ratio of the liquid yields compared to tetralin supports this statement. Table S5 shows the mass balance results and highlights carbon, hydrogen, and oxygen transfer from the coal samples to the liquid yield during tetralin liquefaction at 450

https://doi.org/10.1021/acsomega.4c00602
ACS Omega 2024, 9, 12272−12289

Table 11. Liquefaction Product Distribution of Experiments Conducted at 400, 425, and 450 °C with Tetralin as the Solvent; and 450 °C with Benzene as the Solvent[a]

		abundance, %						
		tetralin	naphthalene	alkylated benzenes	bicyclic compounds	PAH's	O-containing HC's	other
temp	sample	132.1 g mol^{-1}	128.1 g mol^{-1}	120.1−142.1 g mol^{-1}	118.1−138.1 g mol^{-1}	168.1−258.1 g mol^{-1}	220.2−258.1 g mol^{-1}	254.0−334.0 g mol^{-1}
450	VRt	54.4	32.8	10.6	1.3	0.2	0.3	0.1
	VRDt	51.2	41.7	4.7	0.0	1.4	0.2	0.8
	IRt	62.1	29.9	7.1	0.0	0.5	0.8	0.0
	IRDt	53.9	35.6	7.3	0.4	1.1	1.3	0.3
425	VRt	72.4	25.1	2.0	0.0	0.0	0.5	0.0
	VRDt	68.5	28.5	0.0	0.0	0.5	0.3	0.4
	IRt	79.9	18.6	1.4	0.0	0.0	0.2	0.0
	IRDt	68.9	29.2	1.6	0.0	0.0	0.2	0.1
400	VRt	88.7	11.3	0.0	0.0	0.0	0.0	0.0
	VRDt	83.3	16.7	0.0	0.0	0.0	0.0	0.0
	IRt	93.9	6.1	0.0	0.0	0.0	0.0	0.0
	IRDt	85.6	14.4	0.0	0.0	0.0	0.0	0.0

[a]Feed materials—VR, VRD, IR, and IRD; liquefaction temperatures—400, 425, and 450°C; solvent used: t−tetralin.

°C. A significant fraction of carbon originating from the feed materials was transferred to the liquid yield, specifically 9.7, 10.0, 5.4, and 7.3 g from the feed materials with carbon contents of 12.5, 15.0, 10.4, and 14.9 g for VR, VRD, IR, and IRD, respectively. Hydrogen transfer from the IR and IRD coal samples was significantly lower compared to that from the VR and VRD coal samples. It can be assumed that the higher aromatic nature of the inertinite-rich coal results in fewer hydrogen transfer reactions, affecting the overall H/C molar ratios of the liquid yields. Compared to the mass transfer results obtained from benzene liquefaction conducted at 450 °C, presented in Table S6, a significantly larger fraction of hydrogen was transferred from the feed material to the liquid yield despite having significantly lower conversion values. Generally, hydrogenation of benzene is a difficult process; however, at high temperatures and pressures, and in the presence of a catalyst, hydrogenation reactions can proceed to produce compounds like 1,3-cyclohexadiene, cyclohexene, and cyclohexane.[41] From these results, it is also evident that a larger fraction of carbon and hydrogen reacted to produce gases during benzene liquefaction experiments conducted on the VR and VRD samples compared to the IR and IRD samples and may be attributed to the presence of more aliphatic compounds in the VR and VRD samples.

The similarities observed during the structural evaluation, discussed in Section 3.3.1, can be supported by insignificant differences obtained from calorific value determinations. Calorific values were determined on the liquid products from tetralin liquefaction conducted at 450 °C. The results showed that similar values were obtained from the liquids/oils produced from the VR, VRD, IR, and IRD coals, having calorific values of 42.3, 42.8, 42.1, and 42.1 MJ kg^{-1}, respectively. The results can, however, be more qualitatively and semiquantitatively characterized using GC-MS, as presented in Table 11.

The dehydrogenation of tetralin to form naphthalene shows a linear trend in carbon conversion values at increasing liquefaction temperatures, as presented in Table 3. The main products from the liquefaction process were naphthalene, with some fractions of alkylated benzenes and/or tetralin derivatives. The presence of hydrocarbons in the oil samples can be mostly related to the dehydrogenation of tetralin, but can also be a result of the dissolution of organic compounds from the coal samples in tetralin during liquefaction.[17] It can be observed that the breakdown of the coal's macromolecular structure is enhanced at 450 °C, where a higher fraction of alkylated benzenes, polyaromatic hydrocarbons, and oxygen-containing hydrocarbons are produced, with a lower fraction of naphthalene. The results also indicate that a 1-to-3 coal-to-solvent ratio was sufficient for hydrogenation during the liquefaction experiment.

The formation of naphthalene through dehydrogenation of tetralin provided the necessary hydrogen needed to form compounds such as butylbenzene and Indane. Through rearrangement, compounds like 1-methylindane, 1-ethenyl-3-ethylbenzene, 2-methyl-1-propenylbenzene, and 1-phenyl-1-butene could be produced at elevated temperatures. However, the reactions to produce some of these compounds could only proceed when hydrogen atoms are available for initiation.[42] Other compounds, predominantly butylbenzene, were formed through hydrogenation reactions during tetralin liquefaction experiments conducted at 450 °C. Similarly, Indane only formed during experiments conducted at 450 °C, while 1-methylindane, 1-ethenyl-3-ethylbenzene, 2-methyl-1-propenylbenzene, and 1-phenyl-1-butene production started at 425 °C. The total abundance (%) of these four compounds was 8.1, 4.7, 5.1, and 5.5 for VRt, VRDt, IRt, and IRDt at 450 °C, respectively. At 425 °C, the values were significantly lower with 2.0, 1.9, 1.4, and 2.1 for VRt, VRDt, IRt, and IRDt. The results show that at 400 °C the temperature is too low for the production of these compounds.

Blank experiments conducted using only tetralin showed that no reactions occur at these temperatures and pressures. However, at a high concentration of tetralin, the detector responses might have overlapped, masking the presence of other compounds. It should be noted that the experiments were conducted in an inert environment at elevated pressures. Hooper et al.[42] found that insignificant amounts of naphthalene by dehydrogenation and 1-methylindane by rearrangement formed during low-temperature pyrolysis, e.g., 350 °C. However, from 400 to 450 °C, the predominant product was 1-methylindane with a maximum yield of 5% (by weight) at 450 °C. They also noted the formation of hydrogen and methane at 450 °C, which might have formed from, first,

https://doi.org/10.1021/acsomega.4c00602
ACS Omega 2024, 9, 12272−12289

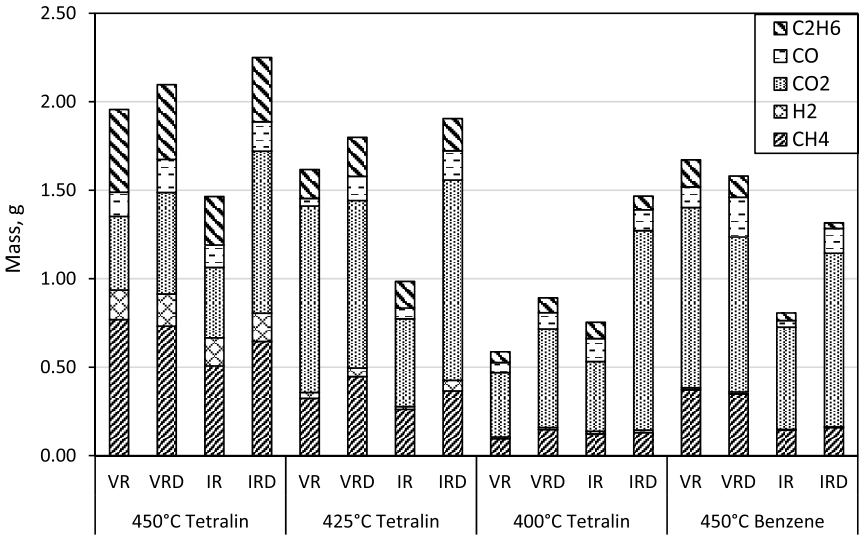


Figure 6. Gas chromatography results of the gas fractions produced from liquefaction experiments.

dehydrogenation reactions, and second, demethylation reactions of 1-methylindane to produce Indane.

Polar and oxygen-containing compounds were absent or in low concentrations in the oil samples. This can be supported by weak alkoxy C−O bands and absent C═O and O−H bands in the FTIR spectra of the oil samples. As reported by Isa et al.,[43] it is favorable to produce residues from liquefaction having low oxygen contents. From this study, it is evident that oxygen-containing functional groups were removed from the coals during the liquefaction process in the form of carbon dioxide and carbon monoxide. This is evident from the gas analysis results presented in Figure 6.

3.4. Gas Analysis − GC-TCD/FID. The data presented in Table S7 include molar/volume percentage values obtained from the gas analysis, along with the corresponding partial pressures of the generated gases. These results served as essential inputs for calculating the masses of compound gases, applying Dalton's law for partial pressure and the Ideal Gas Law. These results are highlighted in Figure 6, showing the mass fractions of the gaseous species obtained from liquefaction experiments conducted at 450 °C using tetralin.

In the liquefaction process, previous research has shown that the primary components of liquefaction gas include hydrogen (H_2), carbon monoxide (CO), carbon dioxide (CO_2), and hydrocarbon compounds such as methane, ethane, and propane.[31] Notably, it has been observed that higher liquefaction temperatures result in an increased production of hydrogen. This phenomenon may be attributed to the thermal breakdown of aliphatic carbon−hydrogen linkages or the cracking of larger molecular compounds at elevated temperatures. Additionally, it is conceivable that the catalyzed dehydrogenation of tetralin is promoted at higher temperatures.

Methane and carbon dioxide start to evolve at relatively low temperatures (200 °C). As the temperature continues to rise, there is internal condensation of the macromolecular structure of low-rank coals. This condensation process initiates the evolution of carbon dioxide (CO_2) and water (H_2O) as byproducts.[31] Decarboxylation reactions were favored at 425 °C to produce CO_2 during liquefaction experiments conducted on all coal samples. When compared to the gas fractions obtained at 450 °C, decarbonylation (and possible dehydration) reactions were favored to produce CO. The reaction of CO_2 and carbon to produce CO may also play a role in the formation of carbon monoxide. The Boudouard reaction demonstrates that at lower temperatures, the equilibrium favors the exothermic production of carbon dioxide, whereas at higher temperatures, the endothermic formation of carbon monoxide becomes the predominant product, as predicted by Le Chatelier's Principle.[31,44]

4. CONCLUSIONS

Liquefaction experiments of inertinite-rich discard coal and vitrinite-rich coal were performed using tetralin and benzene as the solvents. In addition, the demineralized coal fractions were also considered as feed during liquefaction experiments. It was found that inorganic minerals inhibited the liquefaction carbon conversion reactions in the inertinite-rich coal, while promoting conversion reactions in the vitrinite-rich coal. The results indicated that polar functional groups promoted CO and CO_2 formation in the gaseous products at higher liquefaction temperatures. Low concentrations of oxygen-containing functional groups were observed in the liquid and solid residues obtained from the liquefaction experiments. In addition, CO_2 gasification experiments were conducted on the chars of the coals, liquefaction solid residues, and preasphaltenes and asphaltenes (PAA). The gasification results indicated that the conversion reactions were enhanced by inorganic minerals in the inertinite-rich coal char, resulting from higher concentrations of alkaline species compared to the vitrinite-rich coal. Significantly low gasification reactivities were observed for the PAA samples. The results indicated that the solid residues from discard coal fines' liquefaction may be utilized during gasification processes, decreasing the amounts of waste generated and adding economic value to the waste. Lastly, the results from this investigation will aid in the understanding of hydrogen transfer and carbon conversion processes during coliquefaction of inertinite-rich discard coal with plastics such as polypropylene and polyethylene (low-density) using both tetralin and benzene as a solvent.

https://doi.org/10.1021/acsomega.4c00602
ACS Omega 2024, 9, 12272−12289

■ ASSOCIATED CONTENT

Supporting Information

The Supporting Information is available free of charge at https://pubs.acs.org/doi/10.1021/acsomega.4c00602.

Approximated proximate analysis from TGA and calculated higher heating value of solid residues produced from tetralin liquefaction at 425 and 400 °C, and benzene liquefaction at 450 °C, CO_2 gasification reactivities at 960 °C of solid residues produced from tetralin liquefaction at 425 and 400 °C, and benzene liquefaction at 450 °C, RPM- and VRM-derived time factors (t_f), structural parameters (Ψ), quality of fit (QOF), and error sum square (ESS), apparent activation energies (E_a, kJ mol^{-1}) and lumped pre-exponential factors (k_{SO}, min^{-1}) calculated using the different reaction reactivity models from CO_2 gasification experiments of VRD and IRD, and their respective solid residue fractions produced from tetralin liquefaction at 450 °C, mass balance results of the reacting materials and product yields from tetralin liquefaction conducted at 450 °C, mass balance results of the reacting materials and product yields from benzene liquefaction conducted at 450 °C, gas chromatography results of the gas fractions produced from liquefaction experiments, effect of CO_2 gasification temperature on the fractional conversion of the chars from (a) VR, (b) VRD, (c) IR, and (d) IRD, effect of CO_2 gasification temperature on the rate of the reaction as a function of conversion from (a) VR, (b) VRD, (c) IR, and (d) IRD, FTIR spectra of liquid/oil residues obtained from benzene liquefaction conducted at 450 °C on the VR, VRD, IR, and IRD coals, and FTIR spectra obtained from tetralin and benzene (PDF)

■ AUTHOR INFORMATION

Corresponding Author

Naldo J.A. Meyer − *Centre of Excellence in Carbon-Based Fuels, Faculty of Engineering, North-West University, Potchefstroom 2520, South Africa;* orcid.org/0000-0002-3398-4363; Email: 24297070@nwu.ac.za

Authors

Christien A. Strydom − *Centre of Excellence in Carbon-Based Fuels, Faculty of Engineering, North-West University, Potchefstroom 2520, South Africa;* orcid.org/0000-0001-5295-2095

John R. Bunt − *Centre of Excellence in Carbon-Based Fuels, Faculty of Engineering, North-West University, Potchefstroom 2520, South Africa;* orcid.org/0000-0003-3051-2528

Romanus C. Uwaoma − *Centre of Excellence in Carbon-Based Fuels, Faculty of Engineering, North-West University, Potchefstroom 2520, South Africa;* orcid.org/0000-0002-3306-9878

Complete contact information is available at: https://pubs.acs.org/10.1021/acsomega.4c00602

Notes

The authors declare no competing financial interest.

■ ACKNOWLEDGMENTS

The information presented in this paper is based on the research financially supported by the National Research Foundation (NRF) and South African Research Chairs Initiatives (SARChI) of the Department of Science and Technology (Coal Research chair Grant No. 86880). Any opinions, conclusions, or recommendations expressed are those of the author(s), and no liability is accepted on the NRF's regard.

■ REFERENCES

(1) Muzenda, E. Potential uses of South African coal fines: a review. 2014. In *International Conference on Mechanical, Electronics and Mechatronics Engineering*.

(2) Langenhoven, H. *The state of coal mining in South Africa*; Africa, M. C. S., Ed.; Minerals Council: Johannesburg, 2019; p 21.

(3) Ratshomo, K.; Nembahe, R. *South African Coal Sector Report*; Department of Energy: Pretoria, 2017. http://www.energy.gov.za.

(4) Khare, S.; Dell'Amico, M. An overview of conversion of residues from coal liquefaction processes. *Canadian Journal of Chemical Engineering* **2013**, *91* (10), 1660−1670.

(5) Mochida, I.; Okuma, O.; Yoon, S.-H. Chemicals from direct coal liquefaction. *Chem. Rev.* **2014**, *114* (3), 1637−1672.

(6) Burke, F.; Brandes, S.; McCoy, D.; Winschel, R.; Gray, D.; Tomlinson, G. *Summary Report of the DOE Direct Liquefaction Process Development Campaign of the Late Twentieth Century*; National Energy Technology Laboratory (NETL): Pittsburgh, PA, Morgantown, WV, 2001.

(7) Yan, J.; He, J.; Yang, Q.; Bai, Z.; Lei, Z.; Li, Z.; Xue, C.; Wang, Z.; Ren, S.; Kang, S. A study of gasification behavior of residues from mild coal hydro-liquefaction. *Fuel* **2021**, *293*, No. 120456.

(8) Feiner, R.; Schwaiger, N.; Pucher, H.; Ellmaier, L.; Derntl, M.; Pucher, P.; Siebenhofer, M. Chemical loop systems for biochar liquefaction: hydrogenation of naphthalene. *RSC Adv.* **2014**, *4* (66), 34955−34962.

(9) Shalabi, M. A.; Baldwin, R. M.; Bain, R. L.; Gary, J. H.; Golden, J. O. Noncatalytic coal liquefaction in a donor solvent. Rate of formation of oil, asphaltenes, and preasphaltenes. *Industrial & Engineering Chemistry Process Design and Development* **1979**, *18* (3), 474−479.

(10) Schlosberg, R. H. *Chemistry of coal conversion*; Springer Science & Business Media: 1985.

(11) Zhu, X.; Guo, W.; Luo, Z.; Zhu, X.; Cai, W.; Zhu, X. Combined with co-hydrothermal carbonation of wood waste and food waste digestate for enhanced gasification of wood waste. *Fuel* **2023**, *331*, No. 125789.

(12) Guo, Q.; Huang, Y.; He, Q.; Gong, Y.; Yu, G. Analysis of coal gasification reactivity, kinetics, and mechanism with iron-based catalyst from coal liquefaction. *ACS omega* **2021**, *6* (2), 1584−1592.

(13) Uwaoma, R.; Strydom, C.; Matjie, R.; Bunt, J. Gasification of chars from tetralin liquefaction of <1.5 g cm^{-3} carbon-rich residues derived from waste coal fines in South Africa. *J. Therm. Anal. Calorim.* **2022**, *147*, 2353−2367.

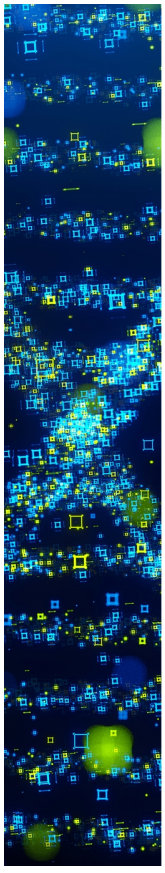
(14) Yan, J.; Bai, Z.; Li, W.; Bai, J. Direct liquefaction of a Chinese brown coal and CO2 gasification of the residues. *Fuel* **2014**, *136*, 280−286.

(15) Bouraoui, Z.; Dupont, C.; Jeguirim, M.; Limousy, L.; Gadiou, R. CO2 gasification of woody biomass chars: The influence of K and Si on char reactivity. *Comptes Rendus Chimie* **2016**, *19* (4), 457−465.

(16) Strydom, C.; Bunt, J.; Schobert, H.; Raghoo, M. Changes to the organic functional groups of an inertinite rich medium rank bituminous coal during acid treatment processes. *Fuel Process. Technol.* **2011**, *92* (4), 764−770.

(17) Uwaoma, R. C.; Strydom, C. A.; Matjie, R. H.; Bunt, J. R. Influence of density separation of selected South African coal fines on the products obtained during liquefaction using tetralin as a solvent. *Energy Fuels* **2019**, *33* (3), 1837−1849.

(18) Parikh, J.; Channiwala, S.; Ghosal, G. A correlation for calculating HHV from proximate analysis of solid fuels. *Fuel* **2005**, *84* (5), 487−494.
(19) Okolo, G. N.; Everson, R. C.; Neomagus, H. W.; Roberts, M. J.; Sakurovs, R. Comparing the porosity and surface areas of coal as measured by gas adsorption, mercury intrusion and SAXS techniques. *Fuel* **2015**, *141*, 293−304.
(20) Şenel, İ. G.; Gürüz, A. G.; Yücel, H.; Kandas, A. W.; Sarofim, A. F. Characterization of pore structure of Turkish coals. *Energy Fuels* **2001**, *15* (2), 331−338.
(21) Horváth, G.; Kawazoe, K. Method for the calculation of effective pore size distribution in molecular sieve carbon. *J. Chem. Eng. Jpn.* **1983**, *16* (6), 470−475.
(22) Kowalczyk, P.; Terzyk, A. P.; Gauden, P. A.; Solarz, L. Numerical analysis of Horvath−Kawazoe equation. *Computers & chemistry* **2002**, *26* (2), 125−130.
(23) Rietveld, H. M. A profile refinement method for nuclear and magnetic structures. *Journal of applied Crystallography* **1969**, *2* (2), 65−71.
(24) Jiang, J.; Yang, W.; Cheng, Y.; Liu, Z.; Zhang, Q.; Zhao, K. Molecular structure characterization of middle-high rank coal via XRD, Raman and FTIR spectroscopy: Implications for coalification. *Fuel* **2019**, *239*, 559−572.
(25) Hirsch, P. B. X-ray scattering from coals. *Proc. R. Soc. London, Ser. A* **1954**, *226* (1165), 143−169.
(26) Everson, R. C.; Okolo, G. N.; Neomagus, H. W.; Dos Santos, J.-M. X-ray diffraction parameters and reaction rate modeling for gasification and combustion of chars derived from inertinite-rich coals. *Fuel* **2013**, *109*, 148−156.
(27) Meyer, J. A.; Strydom, C. A.; Bunt, J. R.; Uwaoma, R. C. Pyrolysis products derived from co-processing of coal fines and microalgae. *Bioresource Technology Reports* **2022**, *19*, No. 101128.
(28) Wen, C. Noncatalytic heterogeneous solid-fluid reaction models. *Industrial & Engineering Chemistry* **1968**, *60* (9), 34−54.
(29) Zhou, H.; Wu, C.; Pan, J.; Wang, Z.; Niu, Q.; Du, M. Research on molecular structure characteristics of vitrinite and inertinite from bituminous coal with FTIR, micro-Raman, and XRD spectroscopy. *Energy Fuels* **2021**, *35* (2), 1322−1335.
(30) Furlong, L.; Effron, E.; Vernon, L.; Wilson, E.Coal processing: the Exxon donor solvent process. *Chem. Eng. Prog.* **1976**, *72*, 8.
(31) Smith, K. L.; Smoot, L. D.; Fletcher, T. H.; Pugmire, R. J. *The structure and reaction processes of coal*; Springer Science & Business Media: 2013.
(32) Smoot, L.; Smith, P. *Coal combustion and gasification*; 1985.
(33) Wang, Z.-C.; Ge, Y.; Shui, H.-F.; Ren, S.-B.; Pan, C.-X.; Kang, S.-G.; Lei, Z.-P.; Zhao, Z.-J.; Hu, J.-C. Molecular structure and size of asphaltene and preasphaltene from direct coal liquefaction. *Fuel Process. Technol.* **2015**, *137*, 305−311.
(34) Kandiyoti, R.; Herod, A.; Bartle, K. D.; Morgan, T. J. *Solid fuels and heavy hydrocarbon liquids: thermal characterization and analysis*; Elsevier: 2016.
(35) Silverstein, R.; Webster, F.; Kiemle, D. *Silverstein-spectrometric identification of organic compounds*, 7th ed.; The State University of New York, College of Environmental Science and Forestry: 2005.
(36) Xie, K. C.; Xie, K. C.; Xie, K.-C.; Xie, K.-C.; Coal gasification. In *Structure and Reactivity of Coal: A Survey of Selected Chinese Coals*; 2015; pp 181−241.
(37) Sakawa, M.; Sakurai, Y.; Hara, Y. Influence of coal characteristics on CO2 gasification. *Fuel* **1982**, *61* (8), 717−720.
(38) Yao, Q.; Ma, M.; Liu, Y.; Ma, D.; Chen, H.; Hao, Q.; Sun, M.; Ma, X. The structural and pyrolysis characteristics of vitrinite and inertinite from Shendong coal and the gasification performance of chars. *Journal of Analytical and Applied Pyrolysis* **2022**, *164*, No. 105519.
(39) Roncancio, R.; Gore, J. P. CO2 char gasification: A systematic review from 2014 to 2020. *Energy Conversion and Management: X* **2021**, *10*, No. 100060.
(40) Everson, R. C.; Neomagus, H. W.; Kaitano, R.; Falcon, R.; Du Cann, V. M. Properties of high ash coal-char particles derived from inertinite-rich coal: II Gasification kinetics with carbon dioxide. *Fuel* **2008**, *87* (15−16), 3403−3408.
(41) Liu, Z.; Liu, S.; Li, Z.; Liu, Z.; Liu, S.; Li, Z.; Liu, Z.; Liu, S.; Li, Z.; Liu, Z.; Liu, S.; Li, Z.Benzene selective hydrogenation thermodynamics, heterogeneous catalytic kinetics catalysis mechanism and scientific essence. In *Catalytic Technology for Selective Hydrogenation of Benzene to Cyclohexene*; 2020; pp 33−57.
(42) Hooper, R. J.; Battaerd, H. A.; Evans, D. G. Thermal dissociation of tetralin between 300 and 450 C. *Fuel* **1979**, *58* (2), 132−138.
(43) Isa, K. M.; Abdullah, T. A. T.; Ali, U. F. M. Hydrogen donor solvents in liquefaction of biomass: A review. *Renewable and Sustainable Energy Reviews* **2018**, *81*, 1259−1268.
(44) Whitehurst, D. D.; Mitchell, T. O.; Farcasiu, M. *Coal liquefaction: the chemistry and technology of thermal processes*; New York, 1980.


CAS BIOFINDER DISCOVERY PLATFORM™
STOP DIGGING THROUGH DATA —START MAKING DISCOVERIES
CAS BioFinder helps you find the right biological insights in seconds
Start your search
CAS
A division of the American Chemical Society

https://doi.org/10.1021/acsomega.4c00602
ACS Omega 2024, 9, 12272−12289